Steel and Composite Structures, *Vol. 34, No. 2 (2020) 241-260*
DOI: https://doi.org/10.12989/scs.2020.34.2.241

Buckling and stability analysis of sandwich beams subjected to varying axial loads

Mohamed A. Eltaher[*1,2] and Salwa A Mohamed[3a]

[1]*Department of Mechanical Engineering, Faculty of Engineering, King Abdulaziz University, P.O. Box 80204, Jeddah, Saudi Arabia*
[2]*Department of Mechanical Design & Production, Faculty of Engineering, Zagazig University,P.O. Box 44519, Zagazig, Egypt*
[3]*Department of Engineering Mathematics, Faculty of Engineering, Zagazig University, P.O. Box 44519, Zagazig, Egypt*

(*Received September 24, 2019, Revised December 2, 2019, Accepted December 12, 2019*)

Abstract. This article presented a comprehensive model to study static buckling stability and associated mode-shapes of higher shear deformation theories of sandwich laminated composite beam under the compression of varying axial load function. Four higher order shear deformation beam theories are considered in formulation and analysis. So, the model can consider the influence of both thick and thin beams without needing to shear correction factor. The compression force can be described through axial direction by uniform constant, linear and parabolic distribution functions. The Hamilton's principle is exploited to derive equilibrium governing equations of unified sandwich laminated beams. The governing equilibrium differential equations are transformed to algebraic system of equations by using numerical differential quadrature method (DQM). The system of equations is solved as an eigenvalue problem to get critical buckling loads and their corresponding mode-shapes. The stability of DQM in determining of buckling loads of sandwich structure is performed. The validation studies are achieved and the obtained results are matched with those. Parametric studies are presented to figure out effects of in-plane load type, sandwich thickness, fiber orientation and boundary conditions on buckling loads and mode-shapes. The present model is important in designing process of aircraft, naval structural components, and naval structural when non-uniform in-plane compressive loading is dominated.

Keywords: sandwich composite; buckling stability; mode-shapes; varying axial load; unified beam theories; Differential Quadrature Method (DQM); convergence of DQM

1. Introduction

Laminated composite structures are made-up from composite materials plies with desirable angle orientations to accomplish desirable and high-performance mechanical properties (i.e., minimum weight with required stiffness and strength properties) for a specified application. Sandwich structures are a special type of composite structures which consist of two thin but strong skins and thick core made up of soft material, Sayyad and Ghugal (2019a). Applications of sandwich composite beam and plate structures have been attractive in many disciplines such as mechanical, marine, military, aerospace, and aeronautical industries. Specially in aerospace industry, sandwich structures are used in landing gear doors, flap track fairings and spoilers, empennages, rudders, winglets, engine environment structures, Li *et al*. (2019). Hence, sandwich structures gained a lot of attention of many researchers and scientists to employ these materials in the design procedures and scientific researches.

Silvestre and Camotim (2002a,b) developed a comprehensive formulation of a generalized beam theory to analyze the structural behavior of composite thin-walled members made of laminated plates and displaying arbitrary orthotropy. Wang and Shenoi (2004) analyzed the buckling of curved sandwich beams with a focus on debonding and buckling/wrinkling of the faces. Meyer-Piening (2006) studied static and buckling of an asymmetric square sandwich plate with orthotropic stiffness properties in the face layers. Silvestre (2007) developed previous model to investigate the buckling behavior of circular cylindrical shells and tubes. Assie *et al*. (2011) developed an effective numerical model to analyze the dynamic time response of orthotropic viscoelastic composite plates. Emam (2011) proved that the classical and first-order theories underestimate the amplitude of buckling while all higher order theories are very close for the static postbuckling response. Eltaher *et al*. (2012, 2013a,b) investigated mechanical responses of functionally graded (FG) nanobeams structures by using differential constitutive form of Eringen model. Basaglia *et al.* (2013) developed a finite element model based on the generalized beam theory to analyze the local, distortional and global post-buckling behavior of thin-walled steel frames. Şimşek and Reddy (2013) studied buckling of a FG microbeam embedded in elastic Pasternak medium by a unified higher order beam theory. Eltaher *et al*. (2014 a,b) modified previous model by considering shear effect to illustrate the mechanical bending, buckling and vibrational behaviors of thick

*Corresponding author, Professor
E-mail: meltaher@kau.edu.sa
[a] Professor
E-mail: sa_mohamed@zu.edu.eg

http://www.techno-press.org/?journal=scs&subpage=6 ISSN: 1229-9367 (Print), 1598-6233 (Online)

nanobeams. Nguyen and Nguyen (2015) and Nguyen *et al.* (2016) presented higher-order shear deformation theory in static, buckling and free vibration analysis of functionally graded (FG) sandwich beams. Meradjah *et al*. (2015) presented a modieid higher order shear and normal deformation theory for FG beams with zero transverse shear stress condition. Emam and Eltaher (2016) investigated buckling and postbuckling of temperature-moisture-dependent composite beams in hygrothermal environments. MalekzadehFard *et al.* (2017) investigated free vibration and buckling of the cylindrical sandwich panel with magneto-rheological fluid layer by improved higher order sandwich panel theory. Kahya and Turan (2018) presented a finite element model based on the first-order shear deformation theory for free vibration and buckling analyses of FG sandwich beams. Mohamed *et al.* (2018) developed a novel numerical differential quadrature procedure to forecast nonlinear forced vibration of curved beam in locality of postbuckling modes. Akbas *et al.* (2018a,b) investigated thermal post-buckling analysis of a laminated composite beam subjected to uniform temperature rise with temperature dependent physical properties. Ebrahimi and Farazmandnia (2018) presented thermo-mechanical buckling of sandwich beams with a stiff core and face sheets made of FG carbon nanotube-reinforced composite within the framework of Timoshenko beam theory. Salami and Dariushi (2018) presented analytical and experimental investigation of geometrically nonlinear analysis of sandwich beams under low velocity impact. Emam et al. (2018) investigated the postbuckling and free vibration behaviors of imperfect composite nanobeams by using nonlocal elasticity differential model of Eringen within the nonlinear Bernoulli-Euler beam theory. Garg and Chalak (2019) presented a comprehensive review on analysis of laminated composite and sandwich structures under hygrothermal conditions. Li *et al*. (2019) examined nonlinear bending of sandwich beams with functionally graded (FG) negative Poisson's ratio honeycomb core in thermal environments by using 3D full scale finite element method (FEM). Martins and Silvestre (2019) analyzed numerically elastic post-buckling behaviour and imperfection sensitivity of simply supported cylindrical steel panels under uniform compression. Chowdhury and Reddy (2019) and Nampally *et al.* (2019) investigated nonlinear deflection of sandwich beams made of architected lattice core by exploited geometrically exact micropolar Timoshenko beam. In the framework of FEM and Rayleigh-Ritz method, Dabbagh *et al*. (2019) studied the influences of nanofllers' aggregation on the vibration frequency of multi-scale hybrid nanocomposites model by trigonometric shear deformation beam theory. Li *et al.* (2019) proposed mixed beam element model for static bending analysis of FG sandwich beam with higher-order shear theories. Sayyad and Ghugal (2019b) developed an analytical solution to investigate static behavior of FG sandwich curved beams by a sinusoidal beam theory. Ascione and Gherlone (2019) exploited the refined zigzag theory to study buckling and nonlinear static response of multilayered composite and sandwich beams. Eltaher *et al.* (2019a) predicted nonlinear postbuckling behaviors of curved carbon nanotube embedded in nonlinear elastic foundation by using modified energy equivalent model. Eltaher *et al.* (2019b) exploited nonlinear integro-partial-differential equation of periodic and aperiodic configuration buckled beam to study nonlinear vibration behaviors of buckled imperfect beam. Mohamed *et al*. (2019) exploited energy equivalent model in analyzing of postbuckling of imperfect carbon nanotubes resting on nonlinear elastic foundation. Chen *et al.* (2019) presented an analytical study on the flexural buckling of sandwich beams considering thermal-induced nonuniform cross-sectional properties. Shen *et al.* (2019) investigated the axial compressive performance of circular concrete-filled steel tubular wrapped by CFRP belts partially by using a nonlinear FEM. Hamed *et al.* (2019) studied effects of porosity models on static behavior of size dependent functionally graded beam. Akbaş (2019) studied post-buckling of laminated composite beams under hygrothermal effect by using FEM. Abdelrahman *et al.* (2019) and Almitani *et al.* (2019) studied free and forced vibration of thin/thick beam structure by using semi-analytical method. Eltaher and Mohamed (2019) illustrated the vibration perforated nanobeams with general boundary conditions by using nonlocal elasticity of Eringen.

Sometimes in real application, sandwich beams are subjected to inplane loads with linear and parabolic distributions, Such as, the load on the stiffened plate in the ship structures, the load applied on the aircraft wings, or the load on the slabs of a multi-storey building, Panda and Ramachandra (2010). So, the performance and response of sandwich beam structures exposed to non-uniform in-plane compressive loading and shear loading is important in aircraft, civil and ship-building industries. Kang and Leissa (2005) and Panda and Ramachandra (2010) studied buckling stability of rectangular plate under linearly varying in-plane loading. Jun *et al.* (2016, 2017) exploited dynamic stiffness method and shear deformation theory to analyze the buckling and free vibration of axially loaded composite laminated beams. Osmani and Meftah (2018) investigated the lateral buckling of tapered thin walled bi-symmetric beams under combined axial and bending loads with shear deformations effects by using Ritz method. Nasrekani and Eipakchi (2019) analyzed static buckling stability of elastic cylindrical shells with varying thickness under combined axial and radial loads under assumption of first-order shear deformation theory. Karamanli and Aydogdu (2019) studied elastic buckling of isotropic, laminated composite and sandwich beams under numerous axially varying in-plane forces based on a modified shear deformable beam theory. Singh and Harsha (2019) used Navier's method to investigate the buckling responses of FGM plate subjected to uniform, linear, and non-linear in-plane loads. Eltaher et al. (2020) studied static stability of a unified composite beams under varying axial loads.

The present study is intended to study the buckling loads and their mode-shapes of composite sandwich laminated beam under varying axial load by using unified beam theories for the first time according to author's knowledge and literature review. The sandwich beam is exposed to axial load with six different distributions, which are uniform load, linear and parabolic loads zero from left

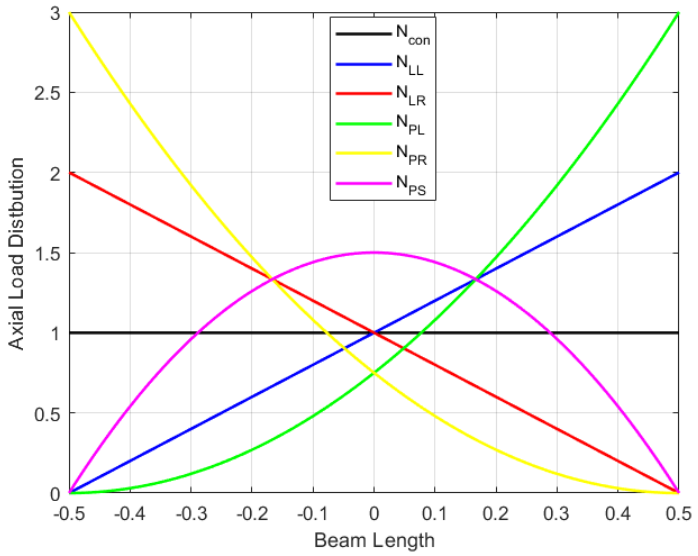

Fig. 1 shows the distribution of the axial in-plane load through the beam length

Table 1 Values of the coefficient of the axial varying load profile

Load Type	Load Symbol	α_2	α_1	α_0
Constant Load	N_{con}	0	0	1
Linear Load-zero from left side	N_{LL}	0	2	0
Linear Load-zero from right side	N_{LR}	0	-2	2
Parabolic Load-zero from left side	N_{PL}	3	0	0
Parabolic Load-zero from right side	N_{PR}	3	-6	3
Symmetric Parabolic Load	N_{PS}	-6	6	0

side, linear and parabolic loads zero from right side, and symmetric parabolic load. Unified higher order beam theories are proposed to consider all slenderness ratios and shear deformation effect of sandwich beam structure. Numerical differential quadrature method (DQM) is exploited to convert the governing equilibrium differential equations into a set of algebraic equations that will be solved after that as an eigenvalue problem. The conversion of DQM in evaluating eigenvalues buckling loads are illustrated in comprehensive form. The manuscript is organized follows: Section 2 presents problem formulation including kinematics assumptions, constitutive equations, axial load functions, and derived equilibrium equations. Section 3 develops the solution procedure and discretization method of the sandwich composite beam structure using numerical differential quadrature method. Model validation and parametric studies are presented and discussed in section 4. Main remarks and conclusion are summarized in section 5.

2. Mathematical formulation

2.1 Axial load distribution

The discrepancy of compressive load along the axial direction has many real applications, such as the stiffened structure of the blend wing, ship structures and multi-storey building. To investigate the behaviors of these structures accurately, the axial compressive load should be described by a uniform function. Hence, in this model the axial compressive load assumed to be varied constant, linear, and parabolic in the axial direction. The function describing the variation of axial load can be stated by Karamanli and Aydogdu (2019)

$$N_{axial}\ (x) = N_{amp}\left[\alpha_2\left(x+\frac{L}{2}\right)^2+\alpha_1\left(x+\frac{L}{2}\right)+\alpha_0\right] = N_{amp}\ C(x) \tag{1}$$

In which N_{amp} is the amplitude of load, that is positive if the load is compressive. The function of axial loads can be adjusted by constant parameters (α_i) of the polynomial described in Eq. (1). The integral of each axially variable in-plane load through the length of the beam is equal to integral of the uniformly distributed in-plane load, to conform results of any profile of load distribution. The value of load profile coefficients described in Eq. (1) are presented in Table 1. The distribution of the axial load through the beam length is presented in Fig. 1.

2.2 Unified theory of sandwich beam

To consider the effect of shear deformation of thick beam, the unified beam theory is proposed. The kinematic displacement field of unified beam theory is described as

$$u_1(x,z,t) = u_0(x,t) - z\frac{\partial w_0(x,t)}{\partial x} + f(z)\varphi(x,t) \quad (2)$$

$$u_3(x,z,t) = w_0(x,t) \quad (3)$$

in which u_1 and u_3 are axial and transverse displacement, respectively, of any point in a beam domain. u_0 and w_0 are the inplane and out of plane displacements along the mid-plane of the beam, respectively. The rotation of the normal to the mid-plane is $\varphi(x,t)$ and $f(z)$ is a shear deformation function along the z-axis, that satisfies the zero shear conditions at the top and bottom lines. The shear distribution along the z-axis can be designated by one of the following functions, Sayyad and Ghugal (2017)

Parabolic shear theory (PST)

$$f(z) = z\left(1 - \frac{4z^2}{3h^2}\right) \quad (3a)$$

Exponential shear theory (EST)

$$f(z) = ze^{-2(z/h)^2} \quad (3b)$$

Trigonometric shear theory (TST)

$$f(z) = \left(\frac{h}{\pi}\right) sin(\pi z/h) \quad (3c)$$

Hyperbolic shear theory (HST)

$$f(z) = h\ sinh(z/h) - z\ cosh(1/2) \quad (3d)$$

The proposed theories eliminate the needing for shear correction factor used in commonly Timoshenko beam theory. The strains accompanying with displacement fields defined by Eqs. (1)-(3) can be described by

$$\varepsilon_x = \frac{\partial u_0}{\partial x} - z - \frac{\partial^2 w_0}{\partial x^2} + f(z)\frac{\partial \varphi}{\partial x} = \varepsilon_x^0 + zk_x^0 + f(z)k_x^2 \quad (4a)$$

$$\gamma_{xz} = \frac{\partial f}{\partial z}\varphi = g(z)k_{xz}^s \quad (4b)$$

in which ε_x is the normal strain along x-direction and γ_{xz} is a shear strain. The other normal $(\varepsilon_y\ ,\varepsilon_z)$ and shear $(\gamma_{xy},\gamma_{yz}\ )$ strain components are zeros.

The constitutive equation along lamina coordinates is described by

$$\begin{Bmatrix} \sigma_x \\ \sigma_y \\ \sigma_{yz} \\ \sigma_{xz} \\ \sigma_{xy} \end{Bmatrix} = \begin{bmatrix} \bar{Q}_{11} & \bar{Q}_{12} & 0 & 0 & \bar{Q}_{16} \\ \bar{Q}_{12} & \bar{Q}_{22} & 0 & 0 & \bar{Q}_{26} \\ 0 & 0 & \bar{Q}_{44} & \bar{Q}_{45} & 0 \\ 0 & 0 & \bar{Q}_{45} & \bar{Q}_{55} & 0 \\ \bar{Q}_{16} & \bar{Q}_{26} & 0 & 0 & \bar{Q}_{66} \end{bmatrix} \begin{Bmatrix} \varepsilon_x \\ \varepsilon_y \\ \gamma_{yz} \\ \gamma_{xz} \\ \gamma_{xy} \end{Bmatrix} \quad (5)$$

At any fiber angle (θ), the transformed reduced stiffnesses can be calculated by

$$\bar{Q}_{11} = Q_{11}\ Cos^4(\theta) + 2[Q_{12} + 2Q_{66}]\ Sin^2(\theta)Cos^2(\theta) + Q_{22}\ Sin^4(\theta) \quad (6a)$$

$$\bar{Q}_{12} = [Q_{11} + Q_{22} - 4Q_{66}]\ Sin^2(\theta)Cos^2(\theta) + Q_{12}\ [Sin^4(\theta) + Cos^4(\theta)] \quad (6b)$$

$$\bar{Q}_{22} = Q_{11}\ Sin^4(\theta) + 2[Q_{12} + 2Q_{66}]\ Sin^2(\theta)Cos^2(\theta) + Q_{22}\ Cos^4(\theta) \quad (6c)$$

$$\bar{Q}_{44} = Q_{44}\ Cos^2(\theta) + Q_{55}\ Sin^2(\theta) \quad (6d)$$

$$\bar{Q}_{55} = Q_{44}Sin^2(\theta) + Q_{55}\ Cos^2(\theta) \quad (6e)$$

$$\bar{Q}_{45} = [Q_{55} - Q_{44}]\ Sin(\theta)\ Cos(\theta) \quad (6f)$$

$$\bar{Q}_{16} = [Q_{11} - Q_{12} - 2Q_{66}]\ Sin(\theta)Cos^3(\theta) + [Q_{12} - Q_{22} + 2Q_{66}]\ Sin^3(\theta)Cos(\theta) \quad (6g)$$

$$\bar{Q}_{26} = [Q_{11} - Q_{12} - 2Q_{66}]\ Sin^3(\theta)Cos(\theta) + [Q_{12} - Q_{22} + 2Q_{66}]\ Sin(\theta)Cos^3(\theta) \quad (6h)$$

$$\bar{Q}_{66} = [Q_{11} + Q_{22} - 2Q_{12} - 2Q_{66}]\ Sin^2(\theta)Cos^2(\theta) + Q_{66}\ [Cos^4(\theta) + Sin^4(\theta)] \quad (6i)$$

The material stiffness constants can be expressed in engineering constants as

$$Q_{11} = \frac{E_1}{1-\vartheta_{12}\vartheta_{21}}\ ,\quad Q_{12} = \frac{\vartheta_{12}E_2}{1-\vartheta_{12}\vartheta_{21}}\ ,\ Q_{22} = \frac{E_2}{1-\vartheta_{12}\vartheta_{21}}\ ,\quad Q_{44} = G_{23}\ ,\ Q_{55} = G_{13}\ ,\ Q_{66} = G_{12} \quad (7)$$

Where E_i , G_{ij} , ϑ_{ij} are the Young modulus, shear modulus, and Poisson's ratio, respectively. Based on unified higher order shear theory, the force resultant (N), the moment resultant (M), unified bending moment resultant (P) and the shear force resultant are defined as

$$\begin{Bmatrix} N \\ M \\ P \\ R \end{Bmatrix} = \begin{bmatrix} A & B & E & 0 \\ B & D & F & 0 \\ E & F & H & 0 \\ 0 & 0 & 0 & F^s \end{bmatrix} \begin{Bmatrix} \varepsilon^0 \\ k^0 \\ k^2 \\ k^s \end{Bmatrix} \quad (8)$$

The laminated in-plane rigidities (A, B, D, E, F, H) and shear rigidity F^s matrices appearing in Eq. (8) are evaluated by the following

$$(A_{ij}\ ,B_{ij}\ ,D_{ij}) = \int_{-h/2}^{h/2} \bar{Q}_{ij}[1\ ,\ z,\ z^2]\ dz \quad (i,j = 1,2,6) \quad (9a)$$

$$(E_{ij}\ ,F_{ij}\ ,H_{ij}) = \int_{-h/2}^{h/2} \bar{Q}_{ij}\ f(z)\ [1\ ,\ z,\ f(z)]\ dz \quad (i,j = 1,2,6) \quad (9b)$$

$$(F_{44}^s\ ,F_{45}^s\ ,F_{55}^s) = \int_{-h/2}^{h/2} g(z) * g(z)\ [\bar{Q}_{44}\ ,\quad \bar{Q}_{45},\quad \bar{Q}_{55}]\ dz \quad (9c)$$

Meanwhile the only nonzero force and moment resultants are N_x, M_x , P_x and R_{xz}, the condensed in-plane force, the bending moment, and unified bending

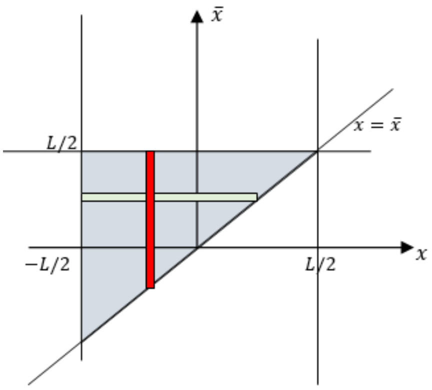

Fig. 2 Domain of the double integral in Eq. (2)

moment can be defined as functions of strain components by

$$\begin{Bmatrix} N_x \\ M_x \\ P_x \end{Bmatrix} = \begin{bmatrix} \bar{A}_{11} & \bar{B}_{11} & \bar{E}_{11} \\ \bar{B}_{11} & \bar{D}_{11} & \bar{F}_{11} \\ \bar{E}_{11} & \bar{F}_{11} & \bar{H}_{11} \end{bmatrix} \begin{Bmatrix} \varepsilon_x^0 \\ k_x^0 \\ k_x^2 \end{Bmatrix} \tag{10}$$

in which

$$\begin{bmatrix} \bar{A}_{11} & \bar{B}_{11} & \bar{E}_{11} \\ \bar{B}_{11} & \bar{D}_{11} & \bar{F}_{11} \\ \bar{E}_{11} & \bar{F}_{11} & H_{11} \end{bmatrix} = \begin{bmatrix} A_{11} & B_{11} & E_{11} \\ B_{11} & D_{11} & F_{11} \\ E_{11} & F_{11} & H_{11} \end{bmatrix} - \begin{bmatrix} A_{12} & A_{16} & B_{12} & B_{16} & E_{12} & E_{16} \\ B_{12} & B_{16} & D_{12} & D_{16} & F_{12} & F_{16} \\ E_{12} & E_{16} & F_{12} & F_{16} & H_{12} & H_{16} \end{bmatrix} \begin{bmatrix} A_{22} & A_{26} & B_{22} & B_{26} & E_{22} & E_{26} \\ A_{26} & A_{66} & B_{26} & B_{66} & E_{26} & E_{66} \\ B_{22} & B_{26} & D_{22} & D_{26} & F_{22} & F_{26} \\ B_{26} & B_{66} & D_{26} & D_{66} & F_{26} & F_{66} \\ E_{22} & E_{26} & F_{22} & F_{26} & H_{22} & H_{26} \\ E_{26} & E_{66} & F_{26} & F_{66} & H_{26} & H_{66} \end{bmatrix}^{-1} \begin{bmatrix} A_{12} & B_{12} & E_{12} \\ A_{16} & B_{16} & E_{16} \\ B_{12} & D_{12} & F_{12} \\ B_{16} & D_{16} & F_{16} \\ E_{12} & F_{12} & H_{12} \\ E_{16} & F_{16} & H_{16} \end{bmatrix} \tag{11}$$

and the shear force can be represented as function of shear strain by

$$R_{xz} = \left(F_{55} - F_{45}^2/F_{44}\right)k_{xz}^s = (\bar{F}_{55})k_{xz}^s \tag{12}$$

2.3 Equilibrium equations

The governing equations can be derived based on the Hamilton's principle as, Meirovitch (2010)

$$\int_{t_1}^{t_2}(\delta T - \delta V + \delta W)dt = 0 \tag{13}$$

In which T, V, and W are the kinetic energy, potential energy, and work done by axial force, respectively. δ denotes the first variation, t_1 and t_2 are arbitrary two instant times. In the current analysis, the problem is static stability of orthotropic composite and hence δT=0.

Based on the unified laminated beam shear theory, the potential energy can be given by

$$V = \frac{b}{2}\int_{-L/2}^{L/2}(N_x\ \varepsilon_x^0 + M_x\ k_x^0 + P_x\ k_x^2 + R_{xz}k_{xz}^s)\,dx \tag{14}$$

Substituting Eqs. (10) and (12) into Eq. (14), the potential energy can be rewritten in terms of strains as

$$V = \frac{b}{2}\int_{-L/2}^{L/2}\Big[(\bar{A}_{11}\varepsilon_x^0 + \bar{B}_{11}k_x^0 + \bar{E}_{11}k_x^2)\ \varepsilon_x^0 + (\bar{B}_{11}\varepsilon_x^0 + \bar{D}_{11}k_x^0 + \bar{F}_{11}k_x^2)\ k_x^0 + (\bar{E}_{11}\varepsilon_x^0 + \bar{F}_{11}k_x^0 + \bar{H}_{11}k_x^2)\ k_x^2 + \left(F_{55} - F_{45}^2/F_{44}\right)k_{xz}^s * k_{xz}^s\Big]\,dx \tag{15}$$

The work done by the axial distributed load is represented by

$$W = \frac{b}{2}\int_{-L/2}^{L/2}\left[N_{axial}\ \left(\int_{-L/2}^{x}\left(\frac{\partial w}{\partial x}\right)^2 dx\right)\right]dx \tag{16}$$

δW of Eq. (16) can't be derived directly and a change of integration order is required. The order of integration can be altered based on the domain shown in Fig. 2.

Hence, by changing the order of integration, the work done can be rewritten as

$$\begin{aligned} W &= \frac{b}{2}\int_{-L/2}^{L/2} N_{axial}\ (\bar{x})\left[\left(\int_{-L/2}^{\bar{x}}\left(\frac{\partial w}{\partial x}\right)^2 dx\right)\right]d\bar{x} \\ &= \frac{b}{2}\int_{-L/2}^{L/2}\left(\frac{\partial w}{\partial x}\right)^2\left(\int_{\bar{x}=x}^{\bar{x}=L/2} N_{axial}\ (\bar{x})\ d\bar{x}\right)dx \\ &= \frac{b}{2}\int_{-L/2}^{L/2} R(x)\left(\frac{\partial w}{\partial x}\right)^2 dx \end{aligned} \tag{17}$$

and the variational form of the work done can be presented as

$$\delta W = b\int_{-\frac{L}{2}}^{\frac{L}{2}} R(x)\left(\frac{\partial w}{\partial x}\right)\ \left(\frac{\partial\ (\delta w)}{\partial x}\right)dx \tag{18}$$

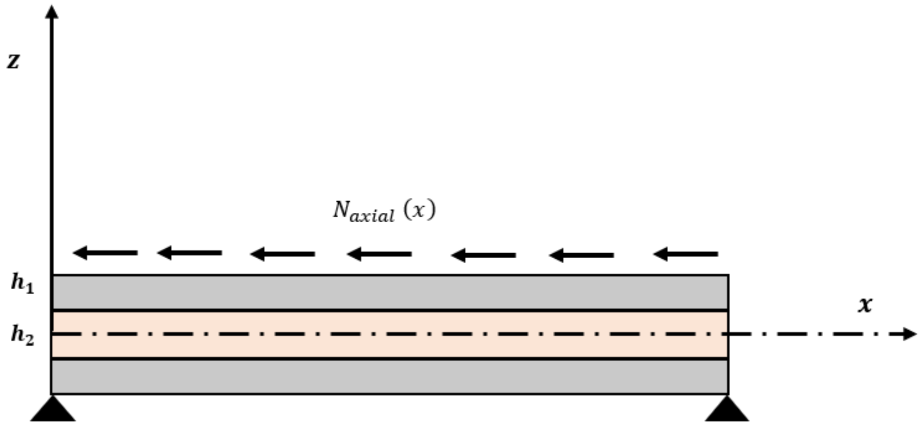

Fig. 3 Geometry of Multilayer Composite beam under the axial distributed loads

$$= b\left[\left[R(x)\left(\frac{\partial w}{\partial x}\right)\delta w\right]_{-L/2}^{L/2} - \int_{-L/2}^{L/2}\left[R(x)\left(\frac{\partial^2 w}{\partial x^2}\right) + \frac{dR(x)}{dx}\left(\frac{\partial w}{\partial x}\right)\right]\delta w\ dx\right]$$

To compute $R(x)$ and $(x)/dx$, substituting Eq. (1) into Eq. (17) and perform integration and then differentiate the results.

$$R(x) = \int_{\bar{x}=x}^{\bar{x}=L/2} N_{axial}\,(\bar{x})\ d\bar{x} = N_{amp}\left(\frac{\alpha_2}{3}L^3 + \frac{\alpha_1}{2}L^2 + \frac{\alpha_0}{2}L - \left(\frac{\alpha_2}{3}\left(x+\frac{L}{2}\right)^3 + \frac{\alpha_1}{2}\left(x+\frac{L}{2}\right)^2 + \alpha_0 x\right)\right) \tag{19}$$

$$\frac{dR(x)}{dx} = -N_{amp}\left(\alpha_2\left(x+\frac{L}{2}\right)^2 + \alpha_1\left(x+\frac{L}{2}\right) + \alpha_0\right) = -N_{amp}\ C(x) \tag{20}$$

Computing the variation of potential energy (V) and substituting the resultant equation and Eq. (18) into variation form of Hamilton Eq. (13), results in governing equilibrium equations of unified sandwich laminated beam under the distributed axial load as

$$\bar{A}_{11}\ u_0'' - \bar{B}_{11}w_0''' + \bar{E}_{11}\varphi'' = 0 \tag{21a}$$

$$\bar{B}_{11}\ u_0''' - \bar{D}_{11}w_0'''' + \bar{F}_{11}\varphi''' + N_{amp}[\ C(x)w_0' - R(x)w_0''] = 0 \tag{21b}$$

$$\bar{F}_{55}\ \varphi - \bar{E}_{11}u_0'' + \bar{F}_{11}w_0''' - \bar{H}_{11}\varphi'' = 0 \tag{21c}$$

subjected to the following boundary conditions

$$[\bar{A}_{11}\ u_0' - \bar{B}_{11}w_0'' + \bar{E}_{11}\varphi']\delta u_0 = 0 \tag{22a}$$

$$[-\bar{B}_{11}\ u_0'' + \bar{D}_{11}w_0''' - \bar{F}_{11}\varphi'' + N_{amp}\ R(x)w_0']\delta w_0 = 0 \tag{22b}$$

$$[-\bar{E}_{11}u_0' + \bar{F}_{11}w_0'' - \bar{H}_{11}\varphi']\delta\varphi = 0 \tag{22c}$$

$$[\bar{B}_{11}\ u_0' - \bar{D}_{11}w_0'' + \bar{F}_{11}\varphi']\delta w_0' = 0 \tag{22d}$$

3. Numerical solution

The governing equilibrium equations (Eq. (21)) of unified laminated sandwich beam under distributed axial load, shown in Fig. 3, are solved by the differential quadrature method DQM.

Let the beam length be discretized by the Chebyshev–Gauss–Lobatto distribution as

$$x_i = -\frac{L}{2} + \frac{L}{2}\left(1 - cos\left(\pi\frac{i-1}{N-1}\right)\right), \qquad i = 1,2,\cdots,N \tag{23}$$

Using the DQM, different order derivatives of a function at a given node can be approximated using a weighted sum of the function values at all discrete nodes in its domain. The first order derivative of function f(x) at node x_i can be approximated using the DQM as follows

$$\left.\frac{df}{dx}\right|_{x=x_i} = \sum_{j=1}^{N} d_{ij}\quad f_j \quad , \quad i = 1,2,\cdots,N \tag{24}$$

where $f_j = f(x_j)$ and d_{ij} denote the corresponding weighting coefficients. The weighting coefficients can be expressed as follows, Shu (2000)

$$d_{ij} = \frac{1}{x_j - x_i}\left(\frac{P_i}{P_j}\right),\quad i \neq j \qquad and \qquad d_{ii} = -\sum_{j=1, j\neq i}^{N} d_{ij} \tag{25}$$

where

$$P_i = \prod_{j=1, j\neq i}^{N}(x_i - x_j),\ i,j = 1,2,\cdots,N \tag{26}$$

In matrix form, let the discrete values of $f_i = f(x_i)$ at different nodes be given as a *vector* $f = [f_1, f_2, \cdots, f_N]^T$. Also, let its first derivative vector be F, then

$$F = \mathcal{D}^{(1)}\ f \tag{27}$$

where $\mathcal{D}^{(1)} = [d_{ij}]$ is the weighting $N \times N$ matrix of the first order derivative. The weighting coefficients matrices for higher-order derivatives can be determined via matrix multiplication. Let the matrices $\mathcal{D}^{(1)}, \mathcal{D}^{(2)}, \mathcal{D}^{(3)}$ and $\mathcal{D}^{(4)}$ be respectively the coefficients matrices corresponding to the first, second, third and fourth derivatives. The unknown variables in Eq. (21) are discretized to three unknown vectors $\mathrm{U} = [u_1, u_2, \ldots, u_i, \ldots, u_N]^T$, $\mathrm{W} = [w_1, w_2, \ldots, w_i, \ldots, w_N]^T$, and $\varphi = [\varphi_1, \varphi_2, \ldots, \varphi_i, \ldots, \varphi_N]^T$ where $u_i = u_0(x_i)$, $w_i = w_0(x_i)$ and $\varphi_i = \varphi_0(x_i)$, $i = 1, 2, \cdots, N$. Also, the given axial load functions $C(x)$ and $R(x)$ appearing in Eq. 19 are discretized respectively as known vectors $\mathrm{C} = [c_1, c_2, \ldots, c_i, \ldots, c_N]^T$ and $\mathrm{R} = [r_1, r_2, \ldots, r_i, \ldots, r_N]^T$.

Accordingly, terms as u_0', w_0''', φ'' are discretized respectively by the vectors $\mathcal{D}^{(1)}\mathrm{U}, \mathcal{D}^{(3)}\mathrm{W}$ and $\mathcal{D}^{(2)}\varphi$. However, to discretize the function ($R(x)w_0'' - C(x)w_0'$) in Eq. 21(b), special matrices multiplications operators are essential. The first is the element by element operator $'\circ'$ defined for matrices $\mathcal{A}, \mathcal{B}$, $\mathcal{C}$ having the same dimensions such that $\mathcal{C} = \mathcal{A} \circ \mathcal{B}$ implies that $\mathcal{C}_{ij} = \mathcal{A}_{ij}\ \mathcal{B}_{ij}$. The second is the vector matrix multiplication operator $'\otimes'$ defined for a vector $\mathcal{V}$ and matrix $\mathcal{A}$ having the same number of rows such that $\mathcal{C} = \mathcal{V} \otimes \mathcal{A}$ implies that $\mathcal{C}_{ij} = \mathcal{V}_i\ \mathcal{B}_{ij}$. The discrete vector of ($R(x)w_0'' - C(x)w_0'$) is given by $\mathrm{V} = \mathrm{R} \circ (\mathcal{D}^{(2)}\mathrm{W}) - \mathrm{C} \circ (\mathcal{D}^{(1)}\mathrm{W})$. Using the operator $\otimes$, this vector can be better written as $\mathrm{V} = (\mathrm{R} \otimes \mathcal{D}^{(2)})\mathrm{W} - (\mathrm{C} \otimes \mathcal{D}^{(1)})\mathrm{W}$ or as $\mathrm{V} = \mathrm{S}\mathrm{W}$ where matrix S is defined by

$$\mathrm{S} = \left(\mathrm{R} \otimes \mathcal{D}^{(2)}\right) - \left(\mathrm{C} \otimes \mathcal{D}^{(1)}\right) \tag{28}$$

The discrete algebraic system corresponding to Eqs. (30) can now be written as

$$\begin{bmatrix} \bar{A}_{11}\mathcal{D}^{(2)} & -\bar{B}_{11}\mathcal{D}^{(3)} & \bar{E}_{11}\mathcal{D}^{(2)} \\ \bar{B}_{11}\mathcal{D}^{(3)} & -\bar{D}_{11}\mathcal{D}^{(4)} & \bar{F}_{11}\mathcal{D}^{(3)} \\ -\bar{E}_{11}\mathcal{D}^{(2)} & \bar{F}_{11}\mathcal{D}^{(3)} & \bar{F}_{55}\mathrm{I} - \bar{H}_{11}\mathcal{D}^{(2)} \end{bmatrix} \begin{bmatrix} \mathrm{U} \\ \mathrm{W} \\ \varphi \end{bmatrix} = N_{amp} \begin{bmatrix} \mathrm{O} & \mathrm{O} & \mathrm{O} \\ \mathrm{O} & \mathrm{S} & \mathrm{O} \\ \mathrm{O} & \mathrm{O} & \mathrm{O} \end{bmatrix} \begin{bmatrix} \mathrm{U} \\ \mathrm{W} \\ \varphi \end{bmatrix} \tag{29}$$

where I is the identity matrix of order N and O is the zero matrix of order $N \times N$. The boundary conditions Eq. (22) are discretized and properly substituted into Eq. (29). The resulting system is a generalized eigenvalue problem that can easily be solved for the eigenvalues (buckling loads) and eigenvectors (mode-shapes). The amplitude of fundamental buckling load N_{amp} is the smallest eigenvalue of the system.

4. Numerical results

The validation, stability of DQM, and parametric studies will be presented through this section in details. First, the validation of the proposed model in analysis of buckling stability of composite laminated structure will be presented in the first subsection to prove the accuracy of this model. After that, the stability of DQM in analysis of buckling loads and mode shapes and the effect of grid points are presented and discussed. The last subsection, effects of load functions, beam theories, slenderness ratio, sandwich ratio, and boundary condition on both buckling stability and buckling modes of sandwich beam will be discussed in comprehensive way. All material data proposed through analysis are $\frac{E_1}{E_2} = varied$; $E_3 = E_2$; $G_{12} = G_{13} = 0.5E_2$; $G_{23} = 0.2E_2$; $\upsilon_{12} = \upsilon_{13} = \upsilon_{23} = 0.25$.

4.1 Validation

The current model is compared with results published by Karamanli and Aydogdu (2019), in which material properties are $\frac{E_1}{E_2} = 25$, $E_3 = E_2$; $G_{12} = G_{13} = 0.5E_2$; $G_{23} = 0.2E_2$; $\upsilon_{12} = \upsilon_{13} = \upsilon_{23} = 0.25$ and geometrical properties are 3 layers with equal thicknesses, total thickness is h, and L/h=20. The dimensionless of first buckling load of symmetric [0°/θ/0°] clamped laminated beam is shown in Table 2, at different loading function and orientation. As concluded form this table, by increasing orientation angle, the critical buckling is decreased. The maximum and minimum critical buckling loads are observed where parabolic load varied from the right N_{PR}, and parabolic load varied from left N_{PL}, respectively. Similar phenomena and identical results (i.e.; within error percentage of 0.5%) are forecast from previous work as present in Table 2.

4.2 DQM convergence

To investigate the convergence behavior of DQM combined with the numerical evaluation of the eigenvalues, several figures are presented to study the effects of orthtropy ratio (E_1/E_2), slenderness ratio (L/h), sandwich ratio (h_2/h_1), and boundary conditions.

The effects of number of grid points N on the numerical results of buckling loads of sandwich structures with different axial load types, different boundary condition and $L = 20h$, $h_2/h_1 = 1$, $E_1/E_2 = 2$ are presented in Table 3. As concluded from table, the results of buckling load is more conformal and stable through grid points $15 \leq N \leq 35$ for this condition. It is observed the maximum deviation for SS, CC, CS, and CF are 0.15%, 0.007%, 0.38% and 5.0%, respectively. The maximum deviation 5% is observed for CF boundary condition at load type of $\boldsymbol{N_{PL}}$ and N=35. A qualitative analysis of Table 3 and mode shapes are presented in Fig. 4. To clarify and simplify analysis, the mode-shapes are evaluated at N=30, however, the buckling load are computed in the full range $15 \leq N \leq 35$ with 2 increment. According to Fig. 4, the mode shapes and critical buckling loads are consistent and stable for the range of grid point $15 \leq N \leq 35$ in case of thin beam $L = 20h$ and small value of orthotropy $E_1/E_2 = 2$.

Table 2 Buckling loads of clamped-clamped symmetric [0°/θ/0°] laminated beam under different axial loads at $\frac{L}{h} = 20$

	Angle	N_{con}	N_{LL}	N_{LR}	N_{PL}	N_{PR}	N_{PS}
Present	0°	47.6967	36.7846	64.0139	33.1590	76.8934	45.5210
	30°	45.7375	35.3262	61.1048	31.8632	73.0642	43.6035
	45°	43.7170	33.8308	58.0637	30.5377	69.0205	41.6204
	60°	41.5712	32.2509	54.8007	29.1402	64.6492	39.5109
	90°	39.2181	30.5249	51.2045	27.6157	59.8270	37.1984
Karamanli and Aydogdu (2019)	0°	47.6910	36.7832	63.9673	33.1581	76.5962	45.5185
	30°	45.7322	35.3248	61.0559	31.8623	72.7507	43.6015
	45°	43.7122	33.8296	58.0117	30.5369	68.6904	41.6192
	60°	41.5672	32.2499	54.7439	29.1395	64.3122	39.5108
	90°	39.2151	30.5241	51.1407	27.6152	59.5063	37.1994

Table 3 Normalized first buckling load for SS, CC using different grid points N ($\boldsymbol{L = 20h}$, $\boldsymbol{h_2/h_1 = 1}$, $\boldsymbol{E_1/E_2 = 2}$)

	SS						CC					
N	Load Type						Load Type					
	N_{con}	N_{LL}	N_{LR}	N_{PL}	N_{PR}	N_{PS}	N_{con}	N_{LL}	N_{LR}	N_{PL}	N_{PR}	N_{PS}
15	17.890	14.801	22.361	13.650	25.647	17.663	68.685	51.950	98.202	46.453	125.733	66.734
17	17.893	14.805	22.359	13.654	25.638	17.667	68.685	51.950	98.201	46.453	125.737	66.733
19	17.897	14.809	22.360	13.658	25.634	17.671	68.685	51.950	98.200	46.453	125.735	66.732
21	17.901	14.813	22.363	13.661	25.633	17.676	68.684	51.950	98.199	46.453	125.734	66.732
23	17.905	14.816	22.366	13.664	25.634	17.680	68.684	51.950	98.198	46.453	125.732	66.731
25	17.908	14.819	22.368	13.667	25.635	17.683	68.684	51.950	98.198	46.453	125.732	66.731
27	17.910	14.821	22.370	13.669	25.635	17.685	68.684	51.950	98.198	46.453	125.731	66.731
29	17.912	14.822	22.371	13.670	25.635	17.686	68.684	51.950	98.198	46.453	125.730	66.731
31	17.912	14.823	22.371	13.670	25.635	17.687	68.684	51.950	98.198	46.453	125.731	66.731
33	17.913	14.823	22.371	13.671	25.634	17.688	68.684	51.951	98.198	46.452	125.730	66.729
35	17.913	14.824	22.370	13.671	25.633	17.688	68.683	51.950	98.198	46.453	125.730	66.730
	CS						CF					
15	49.376	36.535	73.698	32.165	96.193	49.114	7.890	5.212	15.696	4.345	26.557	8.488
17	49.351	36.525	73.628	32.162	96.108	49.072	7.835	5.164	15.693	4.293	26.554	8.488
19	49.330	36.516	73.571	32.160	96.027	49.039	7.787	5.121	15.689	4.249	26.528	8.488
21	49.314	36.509	73.528	32.157	95.964	49.013	7.748	5.089	15.683	4.214	26.485	8.489
23	49.301	36.504	73.495	32.155	95.917	48.994	7.720	5.064	15.681	4.188	26.468	8.488
25	49.293	36.500	73.472	32.154	95.884	48.980	7.701	5.045	15.673	4.168	26.452	8.487
27	49.286	36.497	73.456	32.153	95.862	48.970	7.685	5.031	15.676	4.156	26.395	8.486
29	49.283	36.495	73.446	32.152	95.847	48.964	7.671	5.024	15.662	4.142	26.411	8.495
31	49.280	36.494	73.440	32.152	95.838	48.960	7.668	5.013	15.667	4.138	26.390	8.488
33	49.278	36.494	73.434	32.152	95.834	48.958	7.666	5.015	15.636	4.133	26.405	8.483
35	49.277	36.492	73.435	32.151	95.828	48.955	7.653	5.003	15.632	4.128	26.444	8.476

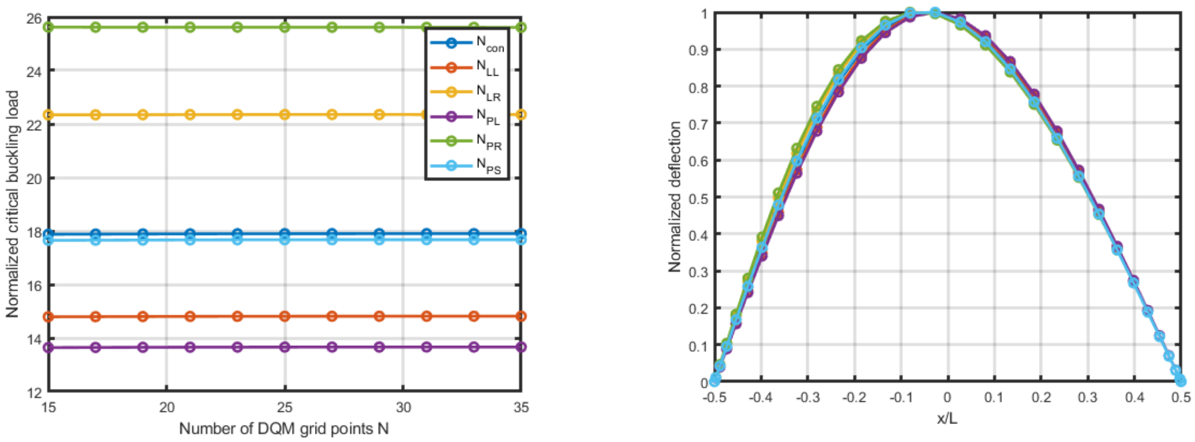

Simply Supported (SS)

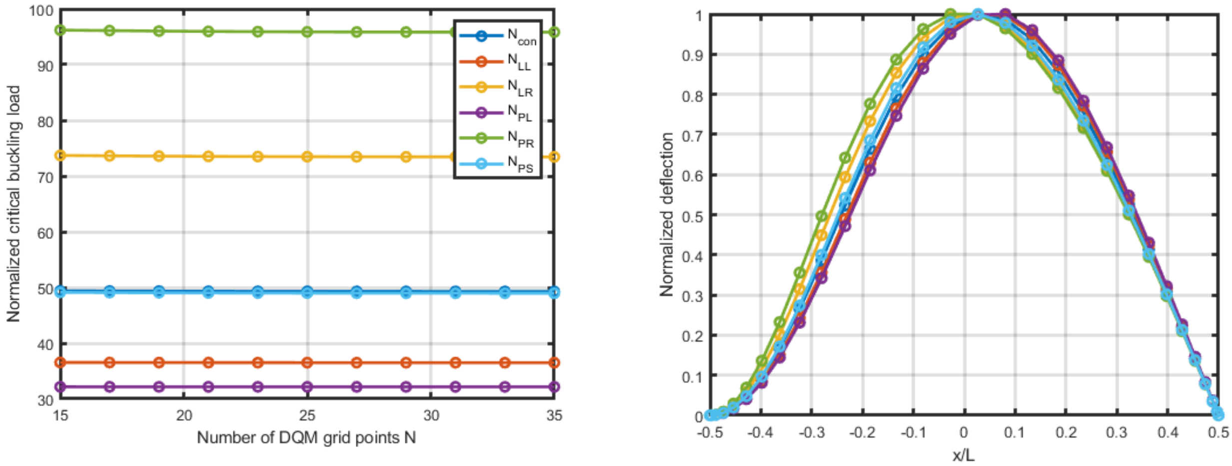

Clamped-Simply (CS)

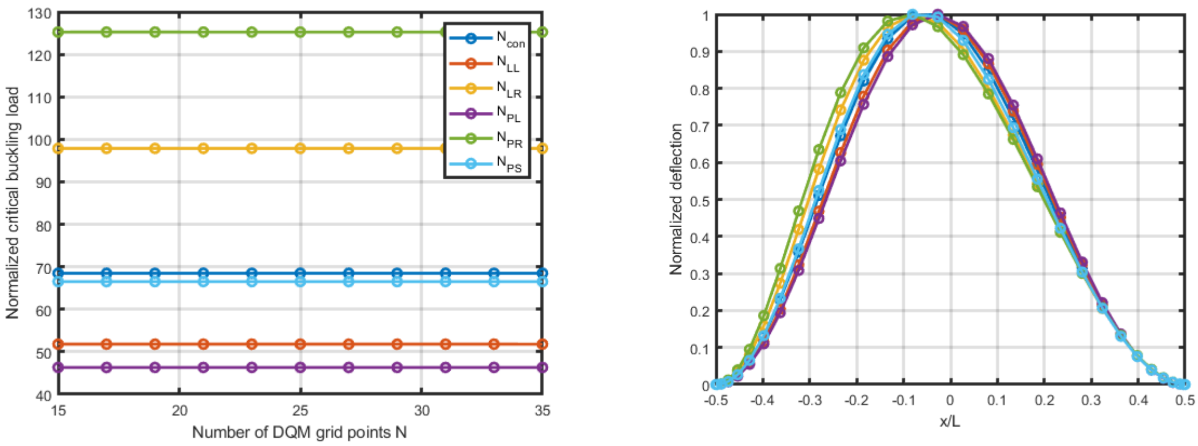

Clamped-Clamped (CC)

Continued-

By changing the orthotropy ratio (E_1/E_2) from 2 to 25, instability analysis is observed in Fig. 5. For a case in hand, the simply supported and clamped free boundary conditions are stable for a whole range of grid points *N*. However, instability in buckling loads and mode shapes are observed for fully clamped and clamped-simply BCs. For example, second buckling mode shapes appears when N=15 in case of CS and CF and oscillations are observed in cases of CC**.** It is found that the stable region of N in buckling analysis for the current case should be $20 \leq N \leq 35$.

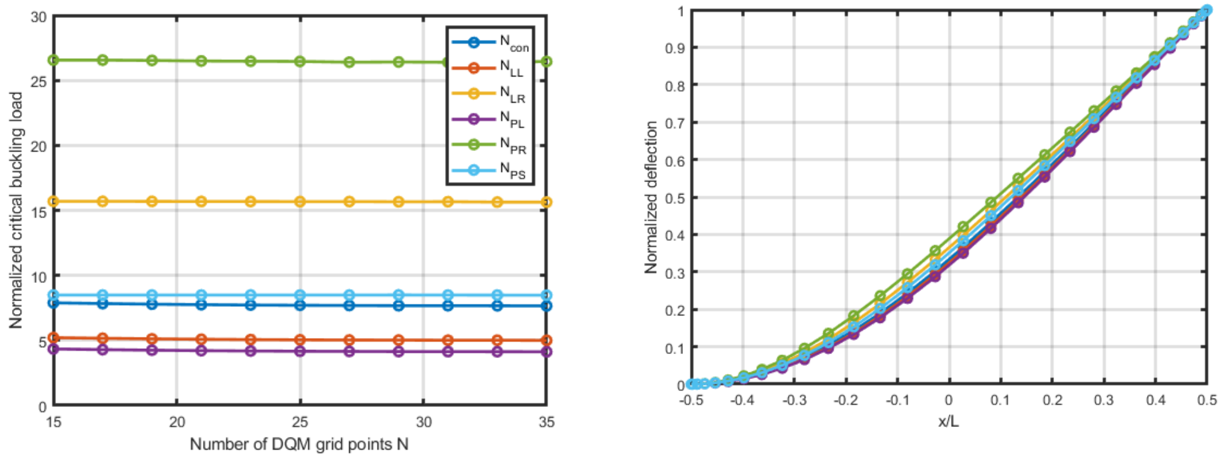

Clamped-Free (CF)

Fig. 4 Convergence analysis of buckling loads and modeshapes of sandwich composite beam. With different boundary conditions at $L = 20h$, $h_2/h_1 = 1,$ $E_1/E_2 = 2$

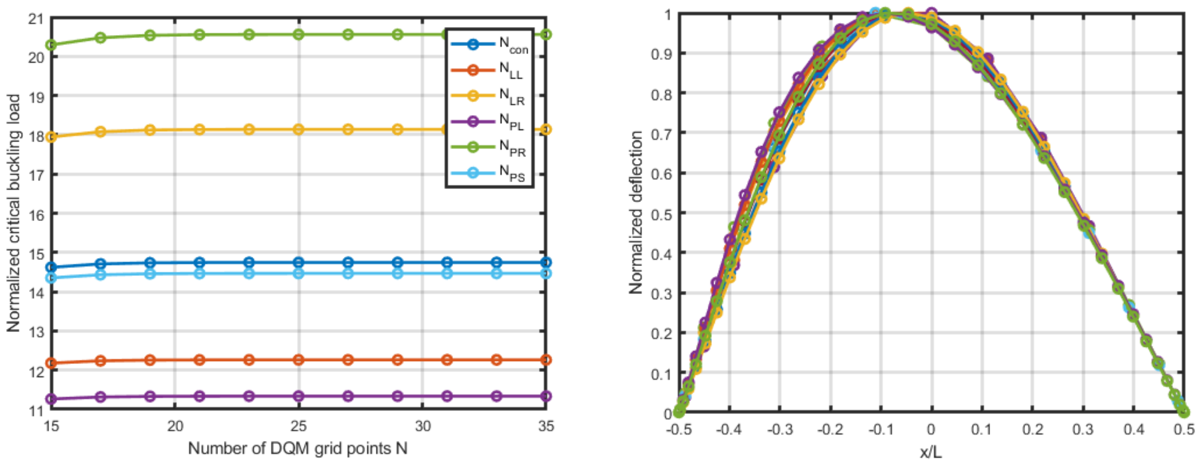

Simply Supported (SS)

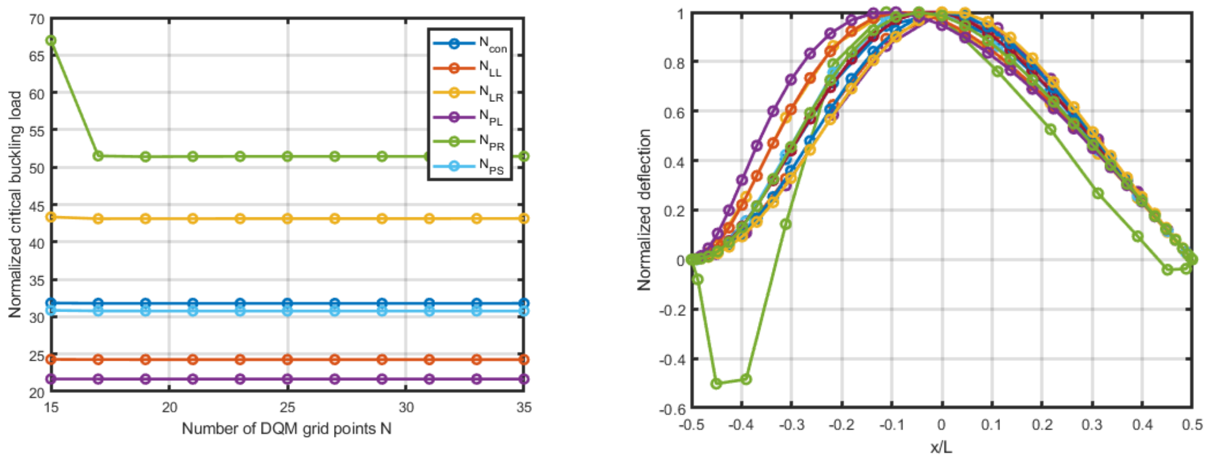

Clamped-Simply (CS)

Continued-

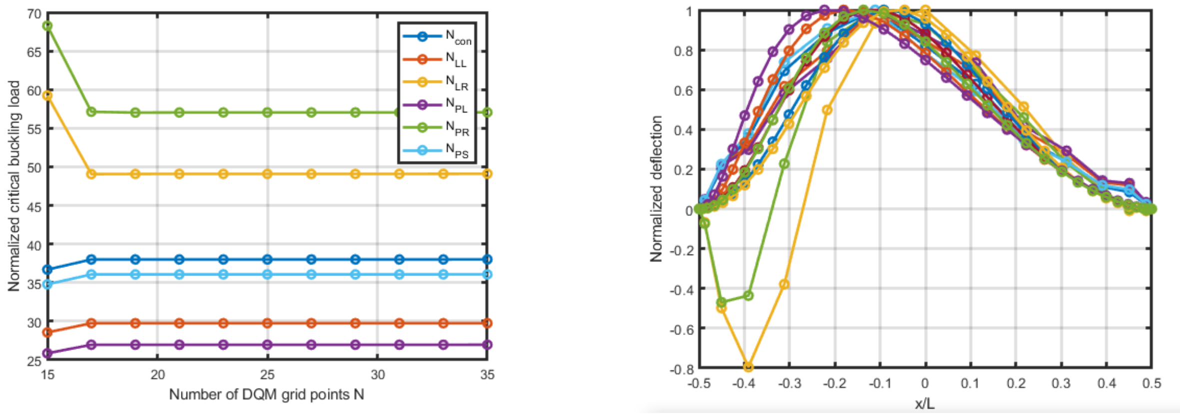

Clamped-Clamped (CC)

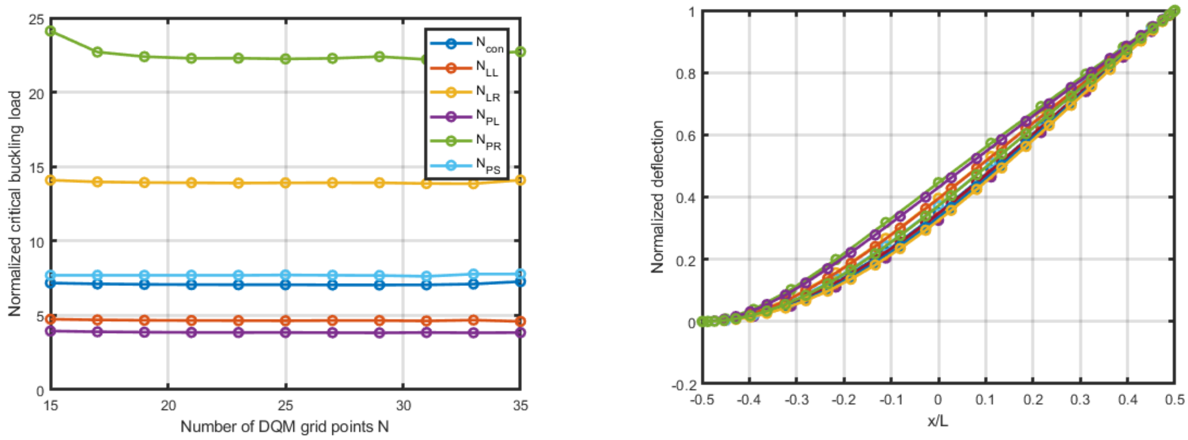

Clamped-Free (CF)

Fig. 5 Convergence analysis of buckling loads and modeshapes of sandwich composite beam. With different boundary conditions at $L = 20h$, $h_2/h_1 = 1,$ $E_1/E_2 = 25$

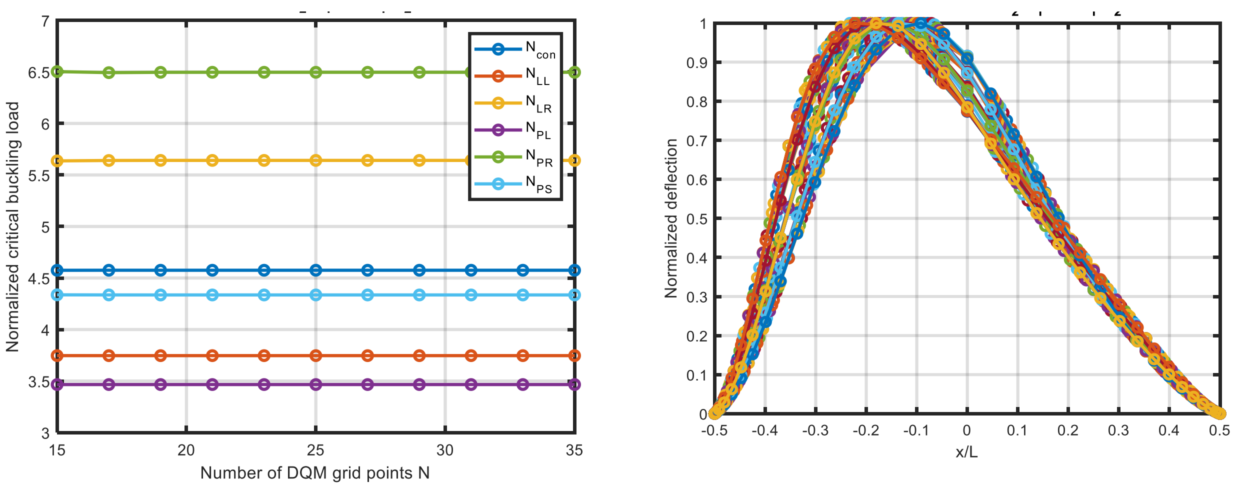

Simply Supported (SS)

Continued-

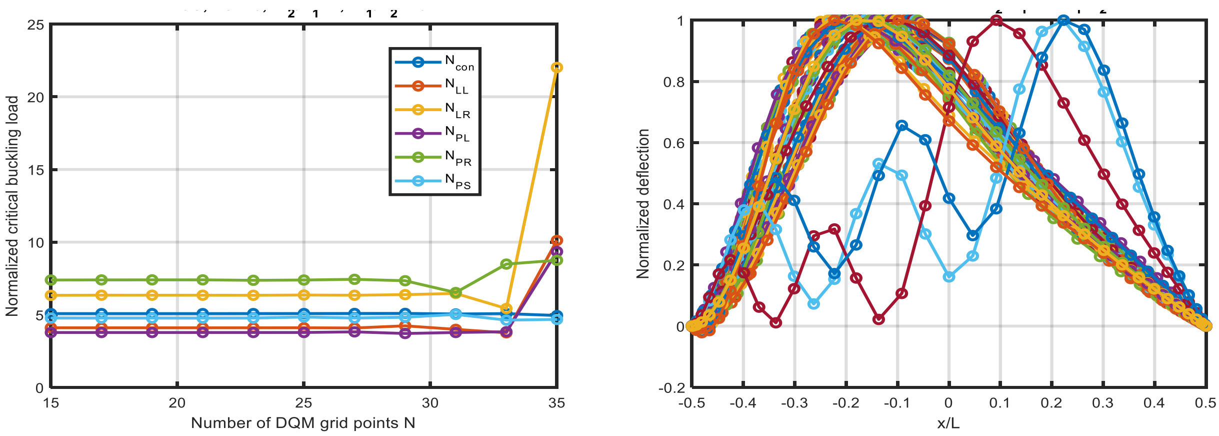

Clamped-Simply (CS)

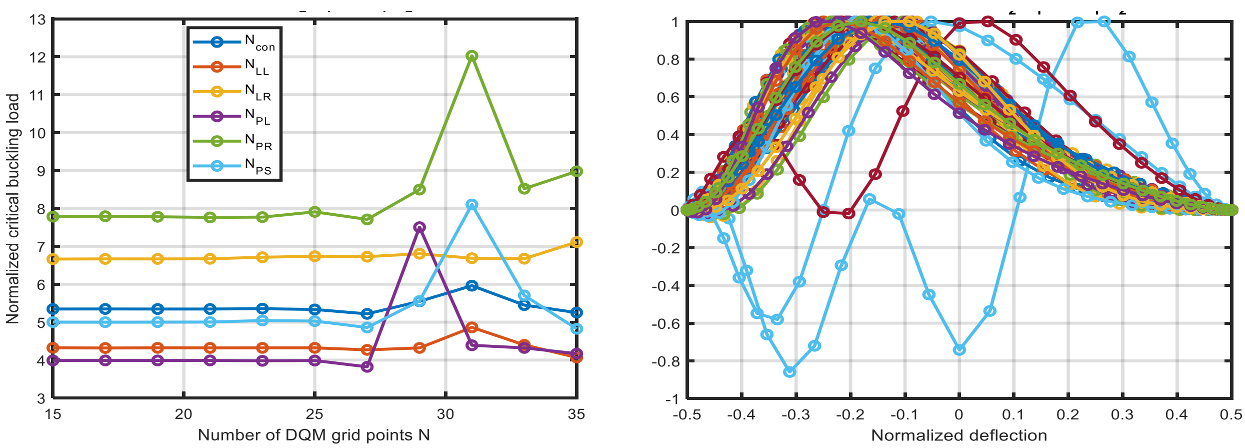

Clamped-Clamped (CC)

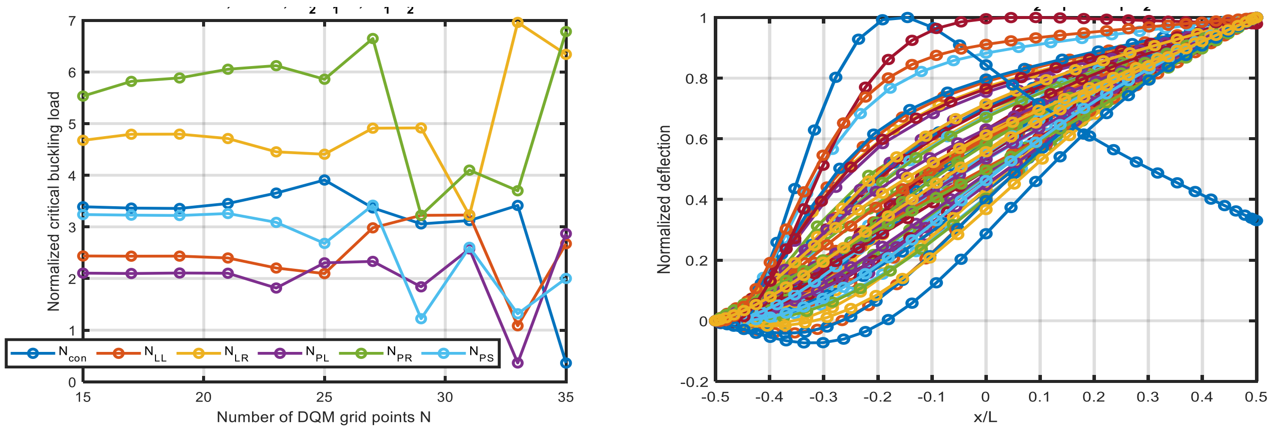

Clamped-Free (CF)

Fig. 6 Convergence analysis of buckling loads and modeshapes of sandwich composite beam. With different boundary conditions at $L = 5h$, $h_2/h_1 = 1$, $E_1/E_2 = 25$

Fig. 6 illustrates the effect of grid points of DQM on the buckling loads and mode shapes for a thick beam $L = 5h$ at $h_2/h_1 = 1$ *and* $E_1/E_2 = 25$. As predicated from previous figure, the buckling analysis of simply supported sandwich beam and associated mode shapes are stable for a full range of DQM grid points. However, instability appears for the other BCs. For CS boundary, the buckling analysis results should be studied with number of grid points less than 30. Over this range, higher order buckling modes exist. To calculate accurate buckling loads and associated mode shape for a thick sandwich CC and CF beams, the grid points of DQM should be less than 25, and 20, respectively.

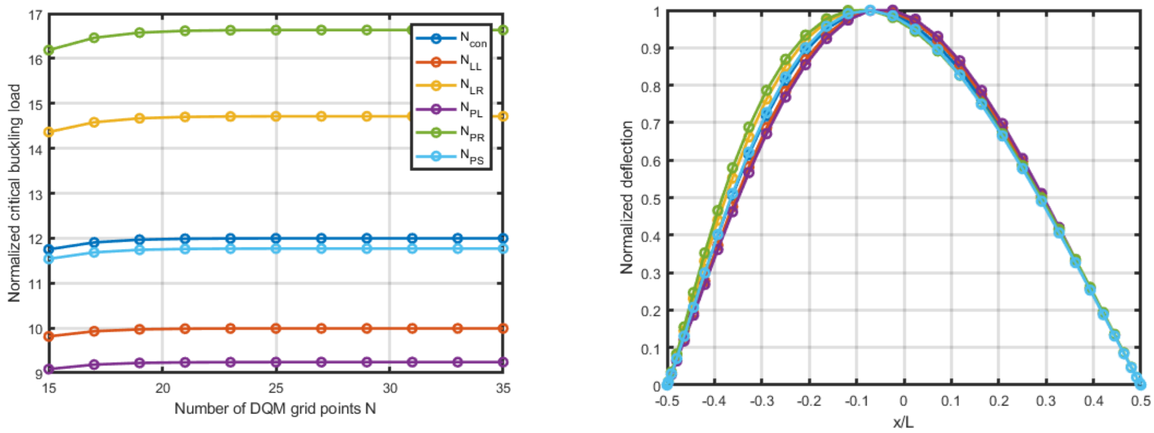

Simply Supported (SS)

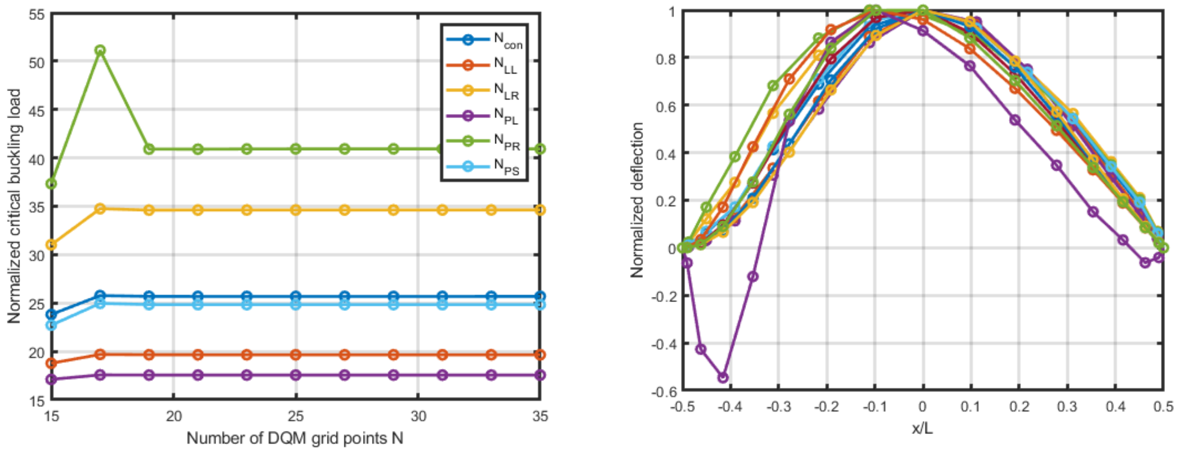

Clamped-Simply (CS)

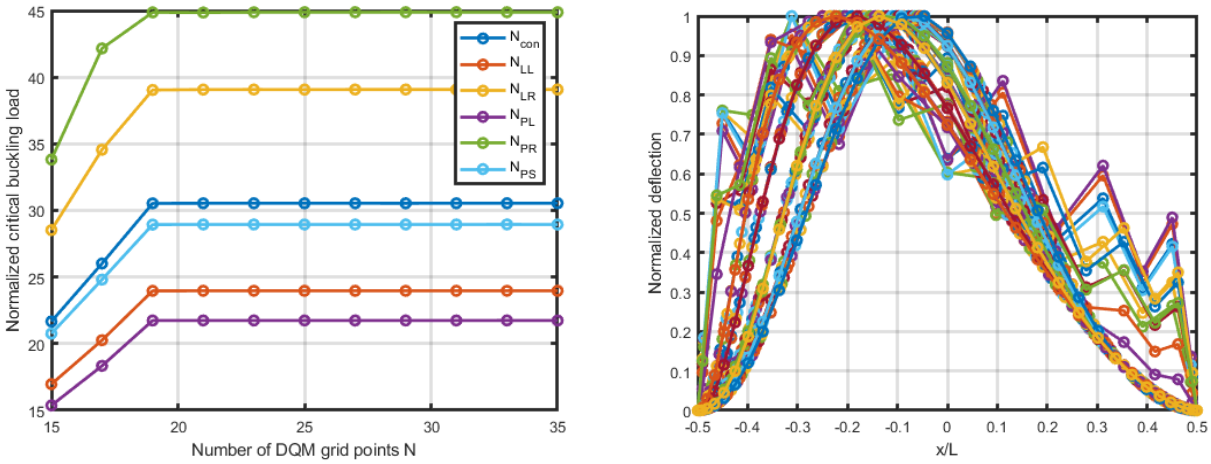

Clamped-Clamped (CC)

Continued-

By comparing Fig. 3 with Figs. 4 and 5, it can conclude that, increasing the orthotropy ratio needs more grid points larger than 20 for accurate results. However, reduction in grid points (less than 20) is required in the case of thick sandwich beam $L = 5h$.

Figs. 7 and 8 illustrate the effect of sandwich ratio on the buckling and mode shape stability and convergence at $L = 20h$ and $E_1/E_2 = 25$. As shown, the numerical results are more significant by changing the sandwich ratio from 1 to 3 or 10 as shown in Figs. 7 and 8. It is clear the simply supported beam is more stable and insensitive to sandwich ratio, slenderness ratio and orthotropy ratio.

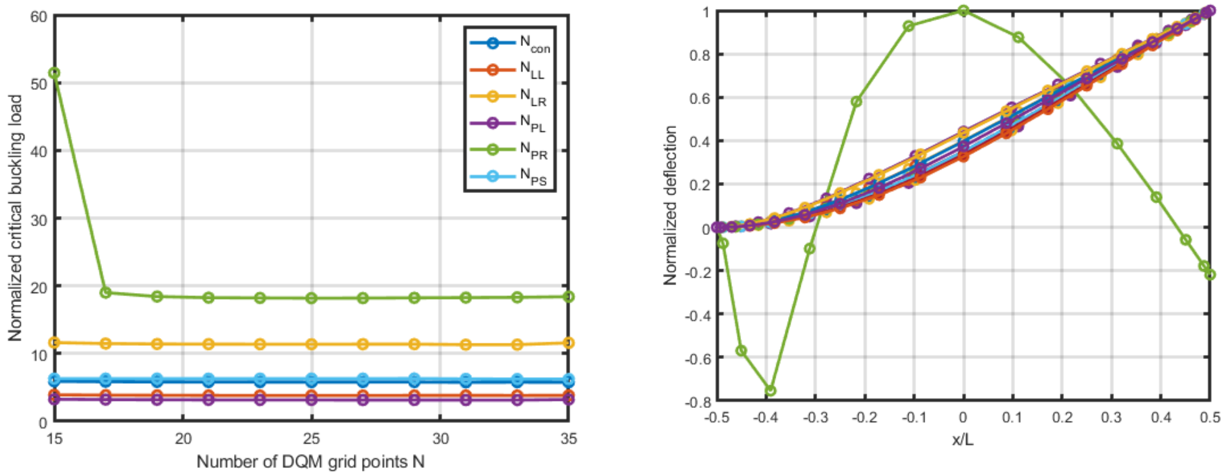

Clamped-Free (CF)

Fig. 6 Convergence analysis of buckling loads and modeshapes of sandwich composite beam. With different boundary conditions at $L = 20h$, $h_2/h_1 = 3$, $E_1/E_2 = 25$

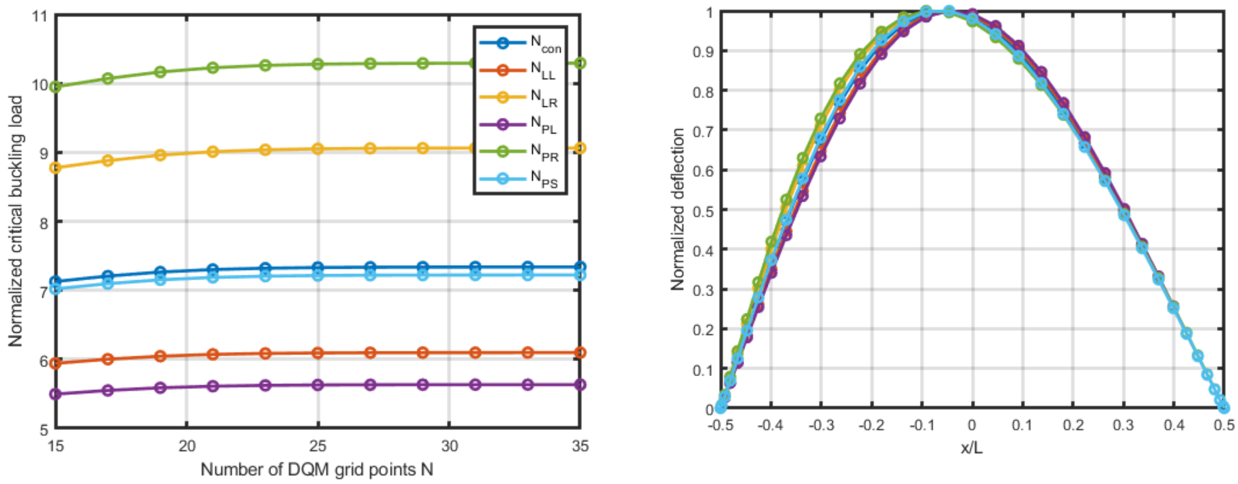

Simply Supported (SS)

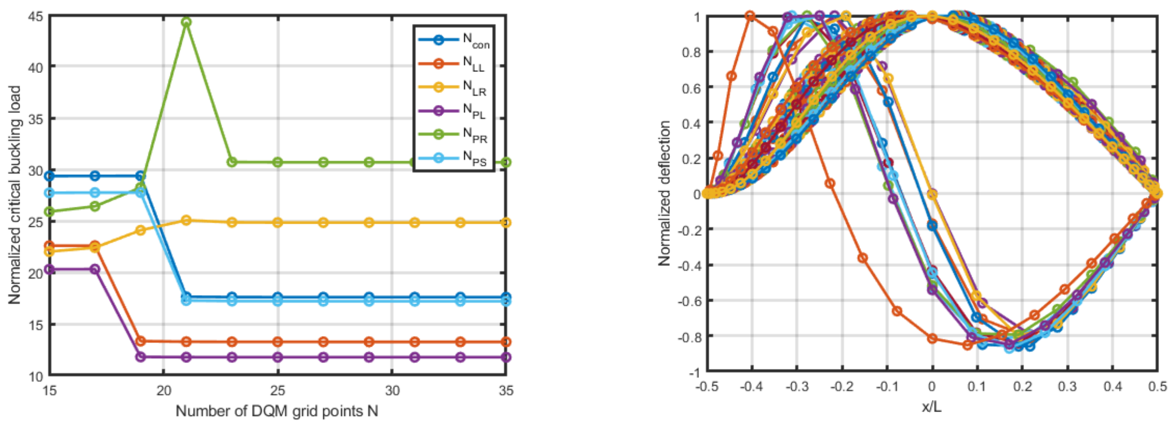

Clamped-Simply (CS)

Continued-

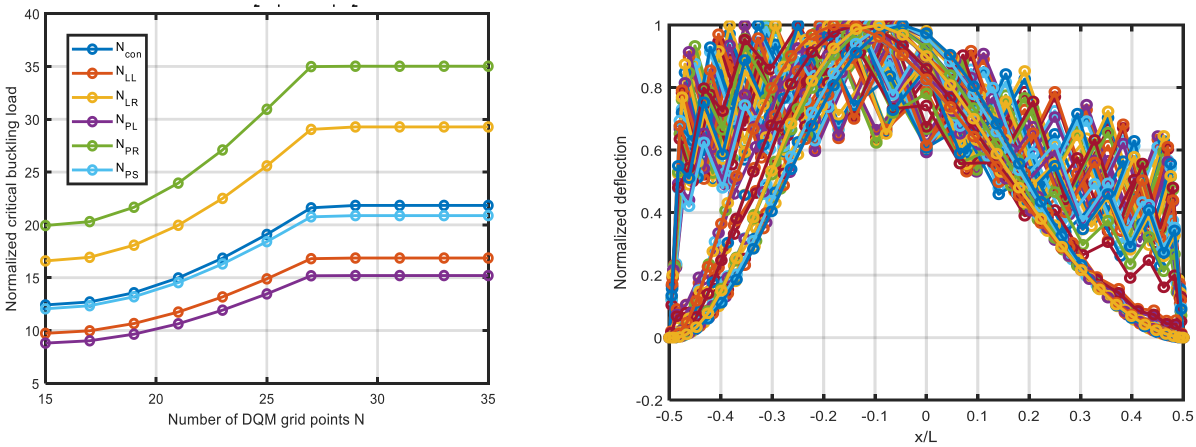

Clamped-Clamped (CC)

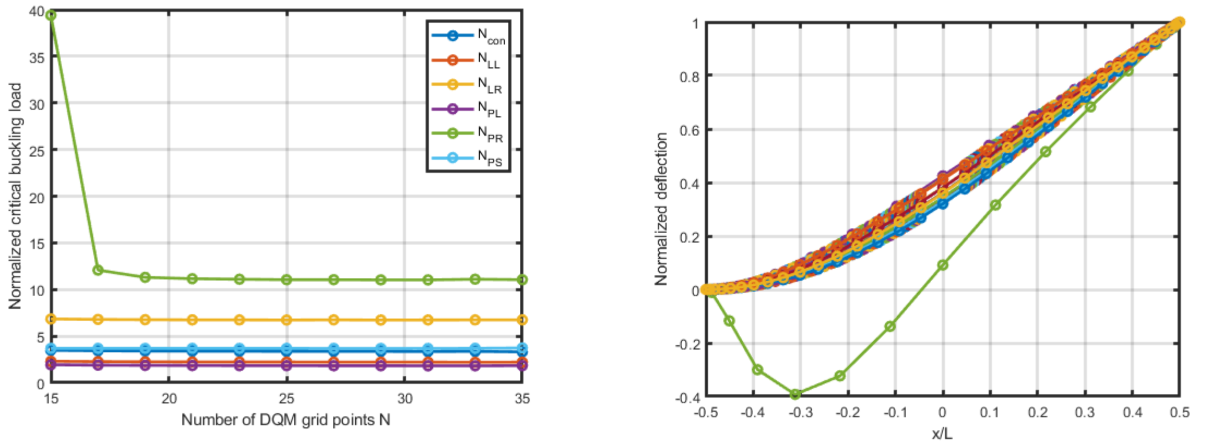

Clamped-Free (CF)

Fig. 7 Convergence analysis of buckling loads and modeshapes of sandwich composite beam. With different boundary conditions at $L = 20h$, $h_2/h_1 = 10$, $E_1/E_2 = 25$

However, the stability and the number of grid points of clamped-clamped boundary condition of sandwich beam are more sensitive to sandwich ratio, slenderness ratio and orthotropy ratio. In case of clamped-simply condition at sandwich ratio $h_2/h_1 = 10$, the instability is observed at the middle grid points of $15 \leq N \leq 35$. It is also observed, results are also depending on the type of loads. Higher mode shape may appear rather than the real modes as illustrated in CS boundary condition (Fig. 7).

4.3 Parametric studies

Through this subsection, the sandwich beam is assumed to be symmetric [0°/90°/0°] and $\boldsymbol{E_1/E_2 = 25}$. The first critical buckling load of sandwich clamped-clamped beam at different beam theories and different loading functions are presented in Table 4. Results in this table are computed by using N=25 for (L/h =20, h_2/h_1 <10), N=35 for (L/h =20, h_2/h_1=10), and N=19 for L/h =5. As shown, the highest buckling load is observed in case of exponential shear theory (EST) and the lowest buckling load is noticed in case of hyperbolic shear theory (HST) for most of slenderness and sandwich ratios. However, in case of $L/h = 20$ and $h_2/h_1 = 1\&3$, the buckling load of HST and EST is the highest one and smallest one, respectively. Which means opposite observation rather than other cases. It is noted that, the buckling loads for PST and HST are very close to each other, even by changing the sandwich ratio h_2/h_1. For all beam theories, the highest buckling is noticed when $\boldsymbol{N_{PR}}$ load is applied, and the smallest buckling load is detected when $\boldsymbol{N_{PL}}$ load is dominated.

Effects of load type and sandwich ratio on the buckling load of clamped-clamped sandwich thin beam with two beam theories are illustrated in Fig. 8. As shown, the buckling load is decreased by increasing the sandwich ratio. This reduction due to increasing the thickness of mid-layer (angle =90°) which has a lesser stiffness than the outer layers (angle =0°). It is also observed that the buckling load is dependent on loading type. As shown, the highest and lowest buckling loads are noticed in case of $\boldsymbol{N_{PR}}$ and N_{PL} , respectively.

Table 4 Dimensionless of 1st buckling load of symmetric $[0°/90°/0°]$ CC COLB_based on different beam shear theories and subjected to different axial in plane loads, $(E_1/E_2 = 25)$

		Beam Theory	N_{con}	N_{LL}	N_{LR}	N_{PL}	N_{PR}	N_{PS}
$L/h = 5$	$h_2/h_1 = 1$	PST	5.3464	4.3222	6.6678	3.9902	7.7799	5.0006
		EST	5.6126	4.4742	7.1649	4.1042	8.4829	5.2866
		TST	5.4826	4.4073	6.9094	4.0386	8.1172	5.1292
		HST	5.3432	4.3211	6.6475	3.9963	7.9008	4.9364
	$h_2/h_1 = 3$	PST	3.8619	3.1690	4.7121	2.9452	5.4283	3.6024
		EST	4.0202	3.2604	4.9920	3.0148	5.8050	3.7561
		TST	3.9342	3.2074	4.8566	2.9713	5.6016	3.6687
		HST	3.8603	3.1664	4.7092	2.9435	5.2984	3.6190
	$h_2/h_1 = 10$	PST	3.1665	2.6795	3.6826	2.5207	4.0953	2.9447
		EST	3.3809	2.8316	3.9821	2.6528	4.4771	3.1467
		TST	3.2664	2.7489	3.8252	2.5807	4.2750	3.0412
		HST	3.1508	2.6797	3.6732	2.5262	4.0816	2.9453
$L/h = 20$	$h_2/h_1 = 1$	PST	38.7107	30.2848	49.9851	27.4408	57.8860	36.7466
		EST	38.0053	29.7512	49.0810	26.9639	57.0413	36.0695
		TST	38.3384	30.0040	49.4968	27.1909	57.4114	36.3888
		HST	38.7475	30.3113	50.0364	27.4648	57.9380	36.7819
	$h_2/h_1 = 3$	PST	30.7555	24.1358	39.3173	21.8929	44.9919	29.1528
		EST	30.5378	23.9676	39.0736	21.7422	44.8773	28.9468
		TST	30.6071	24.0229	39.1322	21.7922	44.8570	29.0115
		HST	30.7720	24.1486	39.3414	21.9041	44.9878	29.1695
	$h_2/h_1 = 10$	PST	21.8417	16.8624	29.2777	15.2030	35.0217	20.8793
		EST	22.1602	17.0911	29.7951	15.4019	35.7775	21.1971
		TST	21.9862	16.9655	29.5119	15.2933	35.3625	21.0208
		HST	21.8299	16.8542	29.2545	15.1949	34.9950	20.8664

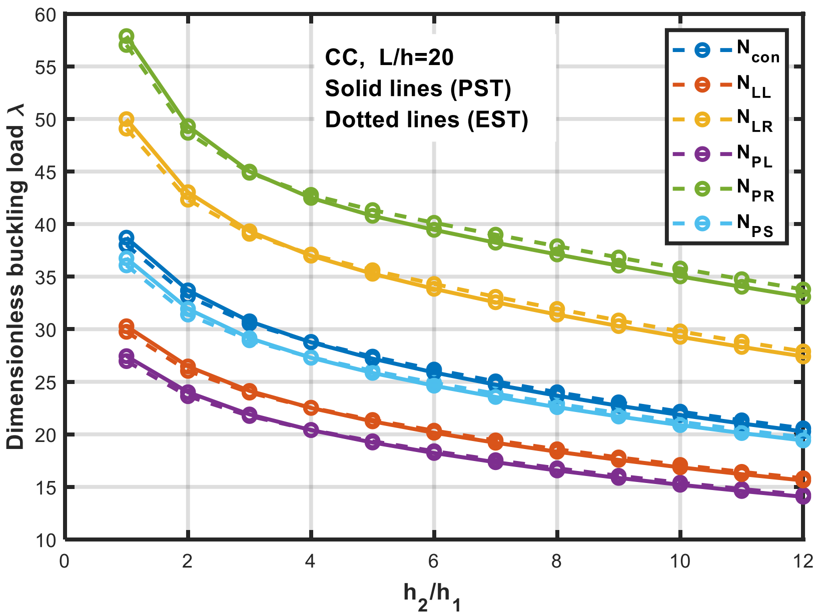

Fig. 8 Effect of sandwich ration on buckling load of clamped-calmped PST and EST at L/h=20

Table 5 Dimensionless of 1st buckling load symmetric [0°/90°/0°] LCBs subjected to different axial in plane loads ($E_1/E_2 = 25$)

		In-plane Load Type						In-plane Load Type					
		N_{con}	N_{LL}	N_{LR}	N_{PL}	N_{PR}	N_{PS}	N_{con}	N_{LL}	N_{LR}	N_{PL}	N_{PR}	N_{PS}
$\frac{h_2}{h_1}\downarrow$	$\frac{L}{h}\downarrow$	**SS Unified (PST)**						**SS Unified (EST)**					
3	5	3.388	2.805	4.105	2.608	4.674	3.199	3.492	2.864	4.290	2.653	4.931	3.303
	10	7.772	6.533	9.274	6.077	10.334	7.502	7.796	6.531	9.359	6.069	10.480	7.522
	20	12.010	10.007	14.717	9.257	16.623	11.784	11.996	9.990	14.713	9.240	16.634	11.768
	50	14.198	11.760	17.692	10.849	20.236	14.012	14.195	11.757	17.689	10.846	20.233	14.008
8	5	2.735	2.315	3.208	2.168	3.564	2.592	2.863	2.407	3.394	2.249	3.797	2.716
	10	5.860	4.930	7.003	4.582	7.780	5.696	5.965	5.009	7.158	4.651	7.979	5.800
	20	8.200	6.822	10.097	6.306	11.442	8.065	8.245	6.857	10.163	6.336	11.526	8.110
	50	9.223	7.635	11.508	7.043	13.178	9.105	9.234	7.644	11.524	7.050	13.197	9.116
		CS Unified (PST)						**CS Unified (EST)**					
3	5	3.702	3.032	4.521	2.811	5.193	3.467	3.833	3.106	4.765	2.866	5.530	3.595
	10	11.093	9.092	13.213	8.356	14.723	10.458	11.106	9.050	13.403	8.307	15.080	10.466
	20	25.837	19.760	34.839	17.647	41.138	24.987	25.680	19.646	34.617	17.549	40.933	24.831
	50	38.139	28.322	56.318	24.983	72.821	37.781	38.082	28.283	56.213	24.950	72.663	37.719
8	5	3.096	2.601	3.631	2.433	4.049	2.894	3.276	2.727	3.894	2.541	4.383	3.064
	10	9.526	7.682	11.368	7.000	12.482	9.025	9.805	7.872	11.843	7.163	13.116	9.296
	20	19.108	14.449	26.652	12.845	32.514	18.624	19.306	14.586	27.000	12.963	33.039	18.830
	50	25.212	18.685	37.468	16.467	48.750	25.028	25.260	18.719	37.552	16.496	48.879	25.078
		CC Unified (PST)						**CC Unified (EST)**					
3	5	3.862	3.169	4.712	2.945	5.428	3.602	4.020	3.260	4.992	3.015	5.805	3.756
	10	11.779	9.825	13.807	9.143	15.345	11.005	11.848	9.821	14.084	9.106	15.813	11.074
	20	30.755	24.136	39.317	21.893	44.997	29.153	30.537	23.968	39.073	21.742	44.878	28.947
	50	51.933	39.415	73.430	35.294	92.955	50.295	51.826	39.337	73.254	35.226	92.702	50.187
8	5	3.217	2.713	3.761	2.551	4.199	2.995	3.419	2.857	4.050	2.675	4.563	3.182
	10	10.244	8.507	11.837	7.874	12.921	9.600	10.607	8.754	12.403	8.089	13.650	9.940
	20	23.679	18.347	31.393	16.564	37.114	22.585	24.007	18.582	31.931	16.770	37.900	22.913
	50	34.780	26.339	49.525	23.564	63.150	33.751	34.883	26.413	49.695	23.628	63.398	33.855
		CF Unified (PST)						**CF Unified (EST)**					
3	5	2.646	1.905	3.618	1.656	4.295	2.488	2.634	1.902	3.666	1.665	4.484	2.512
	10	4.602	3.199	8.216	2.714	11.637	5.060	4.783	3.419	8.042	2.817	11.402	4.957
	20	5.832	3.816	11.404	3.167	18.202	6.380	5.812	3.797	11.379	3.153	18.118	6.309
	50	6.166	4.040	12.530	3.335	21.094	6.807	6.160	4.036	12.543	3.330	21.039	6.807
8	5	2.128	1.511	3.004	1.285	3.389	2.054	2.165	1.529	3.137	1.312	3.662	2.111
	10	3.427	2.269	6.133	1.814	8.919	3.573	3.271	2.233	6.305	1.832	8.814	3.533
	20	3.816	2.513	7.653	2.070	12.369	4.188	3.821	2.509	7.643	2.077	12.464	4.197
	50	3.989	2.613	8.091	2.160	13.667	4.394	3.985	2.612	8.109	2.158	13.667	4.396

A complete comparison between parabolic shear theory and exponential shear theory with different slenderness ratio, sandwich ration and boundary conditions are presented in Table 5. These results are computed using N=29 for L/h=10, 20, 50 and N=19 for L/h=5. As presented in this table, the two beam theories are very close to each other for different slenderness ratio and sandwich ratio at specific load type and boundary conditions.

5. Conclusions

This manuscript presented a comprehensive study of static stability buckling loads and mod-shapes of composite laminated sandwich beams under distributed in-plane axial load. Six functions are proposed to describe the distribution of compressive load through the axial direction. Unified higher order shear deformation theories are proposed to include the shear effects, extension bending, and rigidity of the beam structure. Numerical differential quadrature method (DQM) with the Chebyshev–Gauss–Lobatto distribution is exploited to solve the govern equilibrium equations and derive the critical buckling loads and their mode-shapes. The stability and conversion of proposed model with different grid discretization points are studies and presented in details. The most finding are:-

- Critical buckling loads and mode shapes are dependent on orthtropy ratio, slenderness ration, sandwich ratio, loading type and boundary conditions.
- The numerical results of critical buckling loads and mode shapes are sensitive to the number of grid points.
- In sometimes, the higher grid points are preferred as in most case. However, the lowest grid points are stable, such as, in case of C-C and C-S in Fig. 6.
- The results of beam theories are conformal and close to each other. However, EST and HST ~~gives~~ give higher and smaller values, respectively, rather than other theories.

Acknowledgments

This work was funded by the Deanship of Scientific Research (DSR), King Abdulaziz University, Jeddah, under grant No. (DF-062-135-1441). The authors, therefore, acknowledge with thanks DSR technical and financial support.

References

Abdalrahmaan, A.A., Eltaher, M.A., Kabeel, A.M., Abdraboh, A.M. and Hendi, A.A. (2019), "Free and forced analysis of perforated beams", *Steel Compos. Struct.*, **31**(5), 489-502. https://doi.org/10.12989/scs.2019.31.5.489.

Akbas, S.D. (2018a), "Thermal post-buckling analysis of a laminated composite beam", *Struct. Eng. Mech.*, **67**(4), 337-346. https://doi.org/10.12989/sem.2018.67.4.337.

Akbas, S.D. (2018b), "Post-buckling responses of a laminated composite beam", *Steel Compos. Struct.*, **26**(6), 733-743. https://doi.org/10.12989/scs.2018.26.6.733.

Akbaş, Ş.D. (2019), "Hygrothermal post-buckling analysis of laminated composite beams", *Int. J. Appl. Mech.*, **11**(01), 1950009. https://doi.org/10.1142/S1758825119500091.

Almitani, K.H., Abdalrahmaan, A.A. and Eltaher, M.A. (2019), "On forced and free vibrations of cutout squared beams", *Steel Compos. Struct.*, **32**(5), 643-655. https://doi.org/10.12989/scs.2019.32.5.643.

Ascione, A. and Gherlone, M. (2018), "Nonlinear static response analysis of sandwich beams using the Refined Zigzag Theory", *J. Sandw. Struct. Mater.*, https://doi.org/10.1177/1099636218795381.

Assie, A.E., Eltaher, M.A. and Mahmoud, F.F. (2011), "Behavior of a viscoelastic composite plates under transient load", *J. Mecha, Sci. Technol.*, **25**(5), 1129. https://doi.org/10.1007/s12206-011-0302-6.

Basaglia, C., Camotim, D. and Silvestre, N. (2013), "Post-buckling analysis of thin-walled steel frames using generalised beam theory (GBT)", *Thin-Wall. Struct.*, **62**, 229-242. https://doi.org/10.1016/j.tws.2012.07.003.

Chen, Z., Li, J., Sun, L. and Li, L.Y. (2019), "Flexural buckling of sandwich beams with thermal-induced non-uniform sectional properties", *J. Build.Eng.*, **25**, 100782. https://doi.org/10.1016/j.jobe.2019.100782.

Chowdhury, S.R. and Reddy, J.N. (2019), "Geometrically exact micropolar Timoshenko beam and its application in modelling sandwich beams made of architected lattice core", *Compos. Struct.*, **226**, 111228. https://doi.org/10.1016/j.compstruct.2019.111228.

Dabbagh, A., Rastgoo, A. and Ebrahimi, F. (2019), "Finite element vibration analysis of multi-scale hybrid nanocomposite beams via a refined beam theory", *Thin-Wall. Struct.*, **140**, 304-317. https://doi.org/10.1016/j.tws.2019.03.031.

Ebrahimi, F. and Farazmandnia, N. (2018), "Thermal buckling analysis of functionally graded carbon nanotube-reinforced composite sandwich beams", *Steel Compos. Struct.*, **27**(2), 149-159. https://doi.org/10.12989/scs.2018.27.2.149.

Eltaher, M.A., Emam, S.A. and Mahmoud, F.F. (2012), "Free vibration analysis of functionally graded size-dependent nanobeams", *Appl. Math. Comput.*, **218**(14), 7406-7420. https://doi.org/10.1016/j.amc.2011.12.090.

Eltaher, M.A., Emam, S.A. and Mahmoud, F.F. (2013a), "Static and stability analysis of nonlocal functionally graded nanobeams", *Compos. Struct.*, **96**, 82-88. https://doi.org/10.1016/j.compstruct.2012.09.030.

Eltaher, M.A., Alshorbagy, A.E. and Mahmoud, F.F. (2013b), "Determination of neutral axis position and its effect on natural frequencies of functionally graded macro/nanobeams", *Compos. Struct.*, **99**, 193-201. https://doi.org/10.1016/j.compstruct.2012.11.039.

Eltaher, M.A., Khairy, A., Sadoun, A.M. and Omar, F.A. (2014a), "Static and buckling analysis of functionally graded Timoshenko nanobeams", *Appl. Math. Comput.*, **229**, 283-295. https://doi.org/10.1016/j.amc.2013.12.072.

Eltaher, M.A., Abdelrahman, A.A., Al-Nabawy, A., Khater, M. and Mansour, A. (2014b), "Vibration of nonlinear graduation of nano-Timoshenko beam considering the neutral axis position", *Appl. Math. Comput.*, **235**, 512-529. https://doi.org/10.1016/j.amc.2014.03.028.

Eltaher, M.A., Mohamed, N., Mohamed, S. and Seddek, L.F. (2019a), "Postbuckling of curved carbon nanotubes using energy equivalent model", *J. Nano Res.*, **57**, 136-157. https://doi.org/10.4028/www.scientific.net/JNanoR.57.136.

Eltaher, M.A., Mohamed, N., Mohamed, S.A. and Seddek, L.F. (2019b), "Periodic and nonperiodic modes on postbuckling and nonlinear vibration of beams attached with nonlinear foundations", *Appl. Math. Model.*, **75**, 414-445.

Eltaher, M.A. and Mohamed, S.A. (2020), "Buckling and stability analysis of sandwich beams subjected to varying axial loads" *Steel Compos. Struct*.

Eltaher, M.A., Mohamed, S.A. and Melaibari, M. (2020), "Static stability of a unified composite beams under varying axial loads", *Thin-Wall. Struct.*, **147**, 106488. https://doi.org/10.1016/j.tws.2019.106488.

Emam, S.A. (2011), "Analysis of shear-deformable composite beams in postbuckling", *Compos. Struct.*, **94**(1), 24-30. https://doi.org/10.1016/j.compstruct.2011.07.024.

Emam, S. and Eltaher, M.A. (2016), "Buckling and postbuckling of composite beams in hygrothermal environments", *Compos. Struct.*, **152**, 665-675.

https://doi.org/10.1016/j.compstruct.2016.05.029.
Emam, S., Eltaher, M., Khater, M. and Abdalla, W. (2018), "Postbuckling and free vibration of multilayer imperfect nanobeams under a pre-stress load", *Appl. Scie.*, **8**(11), 2238.
Garg, A. and Chalak, H.D. (2019), "A review on analysis of laminated composite and sandwich structures under hygrothermal conditions", *Thin-Wall. Struct.*, **142**, 205-226. https://doi.org/10.1016/j.tws.2019.05.005.
Hamed, M.A., Sadoun, A.M. and Eltaher, M.A. (2019), "Effects of porosity models on static behavior of size dependent functionally graded beam", *Struct. Eng. Mech.*, **71**(1), 89-98. https://doi.org/10.12989/sem.2019.71.1.089.
Jun, L., Xiang, H. & Xiaobin, L. (2016), "Free vibration analyses of axially loaded laminated composite beams using a unified higher-order shear deformation theory and dynamic stiffness method", *Compos. Struct.*, **158**, 308-322. https://doi.org/10.1016/j.compstruct.2016.09.012.
Jun, L., Li, J. and Xiaobin, L. (2017), "A spectral element model for thermal effect on vibration and buckling of laminated beams based on trigonometric shear deformation theory", *Int. J. Mech. Sci.*, **133**, 100-111. https://doi.org/10.1016/j.ijmecsci.2017.07.059.
Kang, J.H. and Leissa, A.W. (2005), "Exact solutions for the buckling of rectangular plates having linearly varying in-plane loading on two opposite simply supported edges", *Int. J. Solids Struct.*, **42**(14), 4220-4238. https://doi.org/10.1016/j.ijsolstr.2004.12.011.
Karamanli, A. and Aydogdu, M. (2019), "Buckling of laminated composite and sandwich beams due to axially varying in-plane loads", *Compos. Struct.*, **210**, 391-408. https://doi.org/10.1016/j.compstruct.2018.11.067.
Kahya, V. and Turan, M. (2018), "Vibration and stability analysis of functionally graded sandwich beams by a multi-layer finite element", *Compos. Part B: Eng.*, **146**, 198-212. https://doi.org/10.1016/j.compositesb.2018.04.011.
Li, C., Shen, H.S. and Wang, H. (2019), "Nonlinear bending of sandwich beams with functionally graded negative Poisson's ratio honeycomb core", *Compos. Struct.*, **212**, 317-325.
Li, W., Ma, H. and Gao, W. (2019), "A higher-order shear deformable mixed beam element model for accurate analysis of functionally graded sandwich beams", *Compos. Struct.*, **221**, 110830. https://doi.org/10.1016/j.compstruct.2019.04.002.
MalekzadehFard, K., Gholami, M., Reshadi, F. and Livani, M. (2017), "Free vibration and buckling analyses of cylindrical sandwich panel with magneto rheological fluid layer", *J. Sandw. Struct. Mater.*, **19**(4), 397-423. https://doi.org/10.1177/1099636215603034.
Martins, A.D. and Silvestre, N. (2019), "Modal analysis of the post-buckling behaviour of cylindrical steel panels under compression: Imperfection sensitivity and local2 interaction", *Thin-Wall. Struct.*, **144**, 106345. https://doi.org/10.1016/j.tws.2019.106345.
Meirovitch, L. (2010), Methods of analytical dynamics, *Courier Corporation*
Meyer-Piening, H. R. (2006), "Sandwich plates: Stresses, deflection, buckling and wrinkling loads-A case study", *J. Sandw. Struct. Mater.*, **8**(5), 381-394.
Mohamed, N., Eltaher, M. A., Mohamed, S.A. and Seddek, L.F. (2018), "Numerical analysis of nonlinear free and forced vibrations of buckled curved beams resting on nonlinear elastic foundations", *Int. J. Non-Linear Mech.*, **101**, 157-173. https://doi.org/10.1016/j.ijnonlinmec.2018.02.014.
Mohamed, N., Eltaher, M.A., Mohamed, S.A. and Seddek, L.F. (2019), "Energy equivalent model in analysis of postbuckling of imperfect carbon nanotubes resting on nonlinear elastic foundation", *Struct. Eng. Mech.*, **70**(6), 737-750. https://doi.org/10.12989/sem.2019.70.6.737.
Meradjah, M., Kaci, A., Houari, M.S.A., Tounsi, A. and Mahmoud, S.R. (2015), "A new higher order shear and normal deformation theory for functionally graded beams", *Steel Compos. Struct.*, **18**(3), 793-809. https://doi.org/10.12989/scs.2015.18.3.793.
Nasrekani, F.M. and Eipakchi, H. (2019), "Analytical solution for buckling analysis of cylinders with varying thickness subjected to combined axial and radial loads", *Int. J. Pressure Vessels Piping*, **172**, 220-226. https://doi.org/10.1016/j.ijpvp.2019.03.036.
Nguyen, T.K. and Nguyen, B.D. (2015), "A new higher-order shear deformation theory for static, buckling and free vibration analysis of functionally graded sandwich beams", *J. Sandw. Struct. Mater.*, **17**(6), 613-631. https://doi.org/10.1177/1099636215589237.
Nguyen, T.K., Vo, T.P., Nguyen, B.D. and Lee, J. (2016), "An analytical solution for buckling and vibration analysis of functionally graded sandwich beams using a quasi-3D shear deformation theory", *Compos. Struct.*, **156**, 238-252. https://doi.org/10.1016/j.compstruct.2015.11.074.
Osmani, A. and Meftah, S.A. (2018), "Lateral buckling of tapered thin walled bi-symmetric beams under combined axial and bending loads with shear deformations allowed", *Eng. Struct.*, **165**, 76-87. https://doi.org/10.1016/j.engstruct.2018.03.009.
Panda, S.K. and Ramachandra, L.S. (2010), "Buckling of rectangular plates with various boundary conditions loaded by non-uniform inplane loads", *Int. J. Mech. Sci.*, **52**(6), 819-828. https://doi.org/10.1016/j.ijmecsci.2010.01.009.
Salami, S.J. and Dariushi, S. (2018), "Geometrically nonlinear analysis of sandwich beams under low velocity impact: analytical and experimental investigation", *Steel Compos. Struct.*, **27**(3), 273-283. https://doi.org/10.12989/scs.2018.27.3.273.
Sayyad, A.S. and Ghugal, Y.M. (2017), "A unified shear deformation theory for the bending of isotropic, functionally graded, laminated and sandwich beams and plates", *Int. J. Appl. Mech.*, **9**(1), 1750007. https://doi.org/10.1142/S1758825117500077.
Sayyad, A.S. and Ghugal, Y.M. (2019a), "A unified five-degree-of-freedom theory for the bending analysis of softcore and hardcore functionally graded sandwich beams and plates", *J. Sandw. Struct. Mater.*, https://doi.org/10.1177/1099636219840980.
Sayyad, A.S. and Ghugal, Y.M. (2019), "A sinusoidal beam theory for functionally graded sandwich curved beams", *Compos. Struct.*, **226**, 111246. https://doi.org/10.1016/j.compstruct.2019.111246.
Shen, Q., Wang, J., Wang, Y. and Wang, F. (2019), "Analytical modelling and design of partially CFRP-wrapped thin-walled circular NCFST stub columns under axial compression", *Thin-Wall. Struct.*, **144**, 106276. https://doi.org/10.1016/j.tws.2019.106276.
Silvestre, N. and Camotim, D. (2002a), "First-order generalised beam theory for arbitrary orthotropic materials", *Thin-Wall. Struct.*, **40**(9), 755-789. https://doi.org/10.1016/S0263-8231(02)00025-3.
Silvestre, N. and Camotim, D. (2002b), "Second-order generalised beam theory for arbitrary orthotropic materials", *Thin-Wall. Struct.*, **40**(9), 791-820. https://doi.org/10.1016/S0263-8231(02)00026-5.
Silvestre, N. (2007), "Generalised beam theory to analyse the buckling behaviour of circular cylindrical shells and tubes", *Thin-Wall. Struct.*, **45**(2), 185-198. https://doi.org/10.1016/j.tws.2007.02.001.
Şimşek, M. and Reddy, J.N. (2013), "A unified higher order beam theory for buckling of a functionally graded microbeam embedded in elastic medium using modified couple stress theory", *Compos. Struct.*, **101**, 47-58.

https://doi.org/10.1016/j.compstruct.2013.01.017.
Singh, S.J. and Harsha, S.P. (2019), “Buckling analysis of FGM plates under uniform, linear and non-linear in-plane loading”, *J. Mech. Sci. Technol.*, **33**(4), 1761-1767. https://doi.org/10.1007/s12206-019-0328-8.
Wang, W. and Shenoi, R.A. (2004), “Analytical solutions to predict flexural behavior of curved sandwich beams”, *J. Sandw. Struct. Mater.*, **6**(3), 199-216. https://doi.org/10.1177/1099636204032855.

CC